AI-Generated Incentive Mechanism and Full-Duplex Semantic Communications for Information Sharing

Hongyang Du, Jiacheng Wang, Dusit Niyato, *Fellow, IEEE*, Jiawen Kang, Zehui Xiong, and
Dong In Kim, *Fellow, IEEE*

Abstract—The next generation of Internet services, such as Metaverse, rely on mixed reality (MR) technology to provide immersive user experiences. However, limited computation power of MR headset-mounted devices (HMDs) hinders the deployment of such services. Therefore, we propose an efficient information-sharing scheme based on full-duplex device-to-device (D2D) semantic communications to address this issue. Our approach enables users to avoid heavy and repetitive computational tasks, such as artificial intelligence-generated content (AIGC) in the view images of all MR users. Specifically, a user can transmit the generated content and semantic information extracted from their view image to nearby users, who can then use this information to obtain the spatial matching of computation results under their view images. We analyze the performance of full-duplex D2D communications, including the achievable rate and bit error probability, by using generalized small-scale fading models. To facilitate semantic information sharing among users, we design a contract theoretic AI-generated incentive mechanism. The proposed diffusion model generates the optimal contract design, outperforming two deep reinforcement learning algorithms, i.e., proximal policy optimization and soft actor-critic algorithms. Our numerical analysis experiment proves the effectiveness of our proposed methods.

Index Terms—Semantic communications, incentive mechanism, deep reinforcement learning, full-duplex, Metaverse.

I. INTRODUCTION

The development of computer science and wireless networks has continuously enriched the ways of interaction, social communications, and transactions among users, thus playing an irreplaceable role in daily life [1]. From the users' perspective, three significant waves of technological innovation have been witnessed, i.e., the introduction of personal computers, the Internet, and mobile devices. The fourth wave is currently unfolding based on immersive technologies, such as mixed reality (MR), with the goal of forming a ubiquitous virtual space, i.e., Metaverse [2]. Defined as a collective virtual shared world of value co-creation, Metaverse, which is parallel to the physical world, incorporates different technologies to enhance physical spaces, products, and services, thereby revolutionizing online education, business, remote work, and entertainment.

H. Du, J. Wang, and D. Niyato are with the School of Computer Science and Engineering, Nanyang Technological University, Singapore (e-mail: hongyang001@e.ntu.edu.sg, dniyato@ntu.edu.sg, jcwang_cq@foxmail.com)

J. Kang is with the School of Automation, Guangdong University of Technology, China. (e-mail: kavinkang@gdut.edu.cn)

Z. Xiong is with the Pillar of Information Systems Technology and Design, Singapore University of Technology and Design, Singapore (e-mail: zehui_xiong@sutd.edu.sg)

D. I. Kim is with the Department of Electrical and Computer Engineering, Sungkyunkwan University, South Korea (e-mail: dikim@skku.ac.kr)

Immersive technologies, which benefit from powerful computing and rendering capacities, provide users with a natural augmentation of the real world, allowing individuals to generate avatars and seamlessly experience different services. For instance, users can wear MR equipment such as headset-mounted devices (HMDs) and hold controllers to play virtual battle games, just like the scene in the movie "Ready Player One" as shown in Fig. 1. During the game, the user's position in the physical world and the environmental information of the surrounding physical space are collected by devices such as cameras and transmitted to the Metaverse service provider (MSP). The MSP leverages the obtained information to build a virtual gunfight scene and display it to users. Simultaneously, the MR equipment collects the data that describes the user's motion and posture in real time and updates it to the MSP. Through a similar way, some other applications, such as virtual tourism or AIGC services [3], can also be offered in Metaverse. As stated in [4], more than 84% of consumers around the world are interested in using MR for travel experiences, and 42% believe that augmented reality (AR) and virtual reality (VR) are the future of tourism. The reason is that MR enables users to have more engaged and diverse encounters. For instance, travelers in Metaverse can freely choose their destination or generate virtual objects without being restricted by physical limitations and rules. Furthermore, through human-computer interaction technologies, users can interact with other virtual travelers, tour guides, or even AIGC in Metaverse to achieve an immersive experience.

While the above applications are fascinating, several difficulties need to be addressed. *One of the most representative and urgent problems to be solved is that the computational tasks of MR Head-Mounted Displays (HMDs) are overly heavy.* One reason is that, as each player is relatively independent, the scene displayed to the user through the MR HMD needs to be computed and rendered separately, which consumes a lot of computing and transmission resources. For instance, the virtual battle game depicted in Fig. 1 exemplifies a scenario where subsequent players may be subjected to the same or similar in-game events as the previous players, leading to a repetition of computations and rendering virtual objects. One solution to this challenge is establishing an information-sharing scheme among users. Specifically, the view image, i.e., the real-world scene displayed on the MR HMD, serves as a reference point for detecting safe, walkable areas, also known as free-space information, based on the user's unique view image. By sharing the computation results, such as AIGC, and the view image with other users, the users can avoid repeating

Fig. 1. In "Ready Player One", MR-headset-wearing players run through the streets with controllers in hand. However, they look like characters from the game "Halo" running into battle in the Oasis.

computations by comparing received view images to determine the free-space in their own view images and localizing the AIGC. While the information sharing scheme is a viable solution, transmitting such information among users requires a significant amount of transmission resources, particularly for high-definition view images.

In response to the problems above, this paper presents a full-duplex semantic communications framework that aims to enable an efficient information sharing among users. The proposed framework leverages a semantic coding algorithm to extract semantic features from the view image and then transmits them to other users using full-duplex communication. Users can use the received semantic features to obtain free-space information through lightweight semantic matching instead of performing repeated computations. This significantly reduces the computing resources consumed by each user. Furthermore, the full-duplex transmission of semantic information, which has a smaller data size than the original data, minimizes the transmission resource consumption of users.

Moreover, appropriate incentives must be established to motivate users to share semantic information efficiently and effectively [5], [6]. A straightforward and effective way to achieve this is to have the semantic information receiver (SIR) pay an incentive to the semantic information provider (SIP). Contract theory can be used to model the payment scheme for both parties, maximizing the utility of the SIR while meeting the incentive compatibility (IC) and individual rationality (IR) properties of both parties [7]. However, to solve the optimal contract, the recipient of the semantic information must know various characteristics of the sender, such as the cost per unit of transmit power. Additionally, different wireless transmission conditions, such as transmission distance, small-scale fading channels, and co-channel interference, can affect the optimal contract solution [8]. These multidimensional conditions make it challenging to solve the contract design problem with traditional mathematical methods. Although deep reinforcement learning (DRL)-based solutions can find the contract design without specific environmental parameters, the high state dimension can make reinforcement learning-based approaches challenging to solve or prone to falling into a local optimum [9], [10]. To address the aforementioned problems,

taking inspiration from the recent remarkable achievements of generative artificial intelligence (AI) techniques in content generation, specifically diffusion models, we want to leverage generative AI to generate optimum contract designs. Our contributions are summarized as

- We propose a comprehensive framework for full-duplex device-to-device (D2D) semantic communication that enables efficient synchronization of free-space and semantic information among multiple MR users. Our proposed approach eliminates the need for individual users to compute the positions of virtual objects independently in their field of view.

- Within the proposed framework, we consider the effects of wireless fading and self-interference issues that arise in D2D full-duplex communications, and analyzes their impact on the transmission of semantic information. We derive closed-form expressions for both the bit error probability (BEP) and the achievable rate, which are key performance metrics in evaluating the effectiveness of the full-duplex system.

- To promote the sharing of semantic information among users, we present an incentive mechanism design based on contract theory. Specifically, we utilize generative AI, i.e., diffusion model, to design optimal contracts. To evaluate the effectiveness of the AI-generated incentive mechanism, we conduct the numerical analysis and show that our method outperforms the reinforcement learning-based scheme. *To the best of our knowledge, this is the first paper that uses diffusion model for incentive design.*

The remainder of the paper is organized as follows: In Section II, we review the related work in the literature. In Section III, we introduce the semantic-aware free-space information sharing mechanism and propose an end-to-end full-duplex communication system model under generalized fading channel models. Section IV presents the semantic encoding and matching algorithms. In Section V, we propose the diffusion model-based AI-generated contract algorithm. We then perform sound mathematical analysis of the key performance indicators in D2D wireless communications, i.e., achievable rate and BEP. Section VI presents the experiment results. Finally, Section VII concludes this paper.

II. RELATED WORK

In this section, we provide a brief review of three related techniques, i.e., full-duplex communications, visual simultaneous localization and mapping, and mixed reality-aided Metaverse services.

A. Full-Duplex Communications

The full-duplex communications technique allows users to transmit on the same band simultaneously while receiving [11], [12]. Compared with half-duplex communications, full-duplex communications can further improve spectral efficiency, even doubling it if sufficient self-interference cancellation (SIC) is achieved [13]. Motivated by this performance advantage, many research works have been done [14]. For the

cellular networks covered by full-duplex D2D users with residual self-interference, the authors in [15] developed a stochastic geometry-based tractable analytical paradigm to compute the outage probability and rate. The authors in [16] analyzed the capacity improvement of full-duplex D2D underlying cellular networks, concluding that the capacity improvement of full-duplex D2D communications is more significant than that of half-duplex D2D communication if sufficient self-interference cancellation is achieved. Furthermore, the authors in [17] and [18] investigate full-duplex D2D communication from power control and resource allocation perspectives, respectively. However, work has yet to be done to analyze the performance metrics of full-duplex communication systems considering generalized fading channels and interference effects, i.e., self-interference and co-channel interference with signals of arbitrary paths.

B. Visual Simultaneous Localization and Mapping

The visual simultaneous localization and mapping (SLAM) technique uses data gathered by a camera-equipped platform to build a map of the area around the platform while simultaneously locating it inside the map. For the static environment or an environment with few dynamic elements, several visual SLAM systems have been proposed, such as MonoSLAM [19], ORB-SLAM [20], and DSO [21]. Specifically, MonoSLAM is believed to be the first filter-based approach that brings the SLAM problem from the robotic community into pure vision. For dynamic environments, researchers have also developed many systems [22], [22], [23]. Authors in [22] use the object detection network to obtain prior knowledge about dynamic objects and employ a selective tracking algorithm to process the features of dynamic objects, so as to reduce the pose estimation error. In [23], a step-by-step method is proposed, which consists of object detection and contour extraction, to extract semantic information of dynamic objects in a computationally more efficient way. With the rise of wearable devices and advances of matching and detection algorithms in computer vision, such like SuperPoint [24] and SuperGlue [25], the visual SLAM would benefit more applications, especially in Metaverse. Although promising, new problems, such as efficient and effective wireless information sharing among users, need to be solved urgently.

C. Mixed Reality-Aided Metaverse

MR is a general term for a type of technology, including but not limited to the well-known AR and VR, which can seamlessly integrate and merge 3D content into the user's physical environment [26] and enables users to travel freely between the real world and Metaverse. With the support of MR, the MSP can provide users with more services, including educational services, interventional services, communication services, online entertainment, and so forth. The popular Pokemon G [27] can be considered as a miniature of online game in Metaverse. The game uses GPS to locate the player in the physical world and displays creatures based on the obtained location as if they are in the player's real-world through the mobile device's camera. On this basis, players can
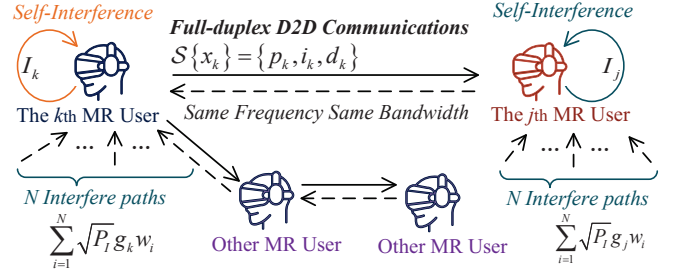

Fig. 2. Device-to-device full-duplex wireless communication system model.

capture, train, and battle the virtual creatures. Although interesting, these systems repeatedly compute and render similar or identical scenes for different players, resulting in a huge waste of computing resources, especially when a large number of players are playing at the same time. Moreover, when different users interact with each other, the transmission of information, particularly the sharing of high-definition images or video streams, also consumes a lot of resources. These problems need to be solved urgently before these systems are further extended into Metaverse.

Motivated by the aforementioned research gaps, we propose a semantic-aware free-space information sharing mechanism to reduce the network resources consumption. To further improve the communication efficiency, the D2D full-duplex techniques is used among users.

III. SYSTEM MODEL

In this section, we present the semantic-aware free-space information sharing mechanism and study a D2D full-duplex communications system.

A. Semantic-Aware Free-Space Information Sharing

When users use an MR technique to access virtual services, e.g., Metaverse, the MR HMDs need to perform various computing tasks. As shown in Fig. 1, HMD devices should compute positions of virtual objects superimposed on the real world, and the planning of routes that users can walk safely in real time. Since even the perspectives of users in the same scene may differ, each user needs to perform the above tasks independently. For example, the kth user generates a virtual flower on the ground, and the jth user, to synchronize this operation, needs to compute where the flower is on the ground according to the jth user's own perspective. A possible solution is to perform user view sharing as shown in Fig. 2. The shared users can obtain the sharer's computation results by view matching without repeating the computation independently. Still with the above example, the kth user can analyze and than share his own view information to other users with similar views, and other users can determine the location of the flower through the view matching. However, the sharing of original view images among MR HMDs consumes a lot of wireless transmission resources, i.e., transmit power and bandwidth. The reason is that the HMD resolution is high, resulting in a large amount of data for view images.
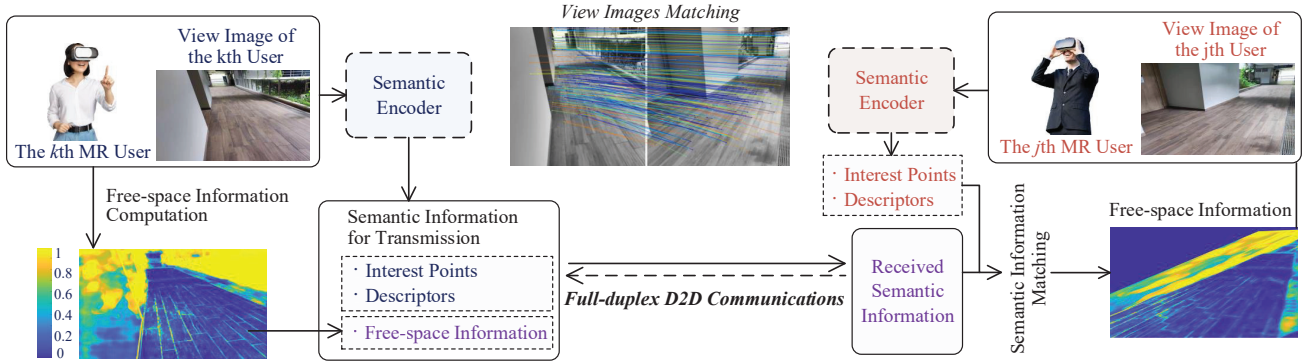
Fig. 3. The semantic-aware free-space information sharing mechanism proposed in this paper. Full-duplex wireless communication is performed between MR HMDs among users. The free-space information is computed by the state-of-art anomaly detection approach named JSR-Net [28]

To solve this problem and achieve efficient and effective information sharing, we apply the semantic communication technique in the D2D full-duplex communication system. A representative task could be *free-space information sharing*. As shown in Fig. 3, specifically, a user who identifies an area in their view image that is safe to walk in can share the detected free-space information with other users. Other users can then directly perform the matching to obtain safe walking area in their own view images. Let $\mathbf{x}_k$ denote the original view image of the kth user. Here the semantic information includes the detected free-space ($\mathbf{i}_k$), the interest points that reflect important structures in the visual field diagram ($\mathbf{p}_k$), and the descriptors corresponding to interest points ($\mathbf{d}_k$). Let $\mathcal{S}\{\cdot\}$ denote the semantic encoder, we have

$$\mathcal{S}\{\mathbf{x}_k\} = \{\mathbf{p}_k, \mathbf{d}_k, \mathbf{i}_k\}. \qquad (1)$$

The total data size of the semantic information, i.e., $\{p_k, d_k, i_k\}$, will be much smaller than that of the original view image, i.e., $\{x_k\}$. The detailed design of the semantic encoder is presented in Section IV-A.

B. Full-Duplex Wireless Communications

Although semantic communication technologies can reduce the amount of data transmitted without affecting task completion, bandwidth resources are still strained when the number of users is large. Because of limited bandwidth resources in the HMD device network, we consider that users are communicating with each other in the full-duplex mode.

A critical issue in full-duplex communication is self-interference cancellation. To investigate the effect of the residual self-interference, i.e., I_k, on system performance, we consider that I_k is subject to the Gaussian distribution [29]. This can be regarded as the worst-case assumption [1] about the interference [30]. Specifically, the residual self-interference at k^{th} user and j^{th} user can be modeled as zero-mean complex Gaussian random variables with variance $\upsilon_k P_k \sigma_S^2$ and $\upsilon_j P_k \sigma_S^2$, respectively [30], where P_k is the transmit power of the kth user and σ_S^2 denotes the variance due to unit power. The parameters υ_k and υ_j are the constants that reflect the

[1]The exact residual self-interference modeling could be different according to the interference cancellation technique, which is left for our future work.

self-interference cancellation abilities of kth user and j^{th} user, respectively [30].

We consider that the jth user is transmitting the semantic information to the kth user. Let s_j denote the transmitted symbol in $\mathcal{S}\{\mathbf{x}_j\}$. The received signal at the kth user can be expressed as

$$y_k = \sqrt{P_j D_{jk}^{-\beta_k}} h_{jk} s_j + \sum_{i=1}^{N} \sqrt{P_I} g_k w_i + I_k + n_k, \qquad (2)$$

where $n_k \sim \mathcal{CN}\left(0, \sigma_N^2\right)$, $I_k \sim \mathcal{CN}\left(0, \upsilon_k P_k \sigma_S^2\right)$, h_{jk} is the small-scale fading channel, P_j is the transmit power of the jth user, D_{jk} is the distance between the kth user and j^{th} user, β_k is the corresponding path loss exponents, N is the number of interfere paths that are assumed to be present at the kth user-j^{th} user full-duplex communications pair, each of the interfering signals has an average transmit power P_I, w_i is the ith interfering symbol, and g_k is the small-scale fading of the interfering signal.

The frequency band used for D2D communications among users is lower than 5 GHz. We consider that the interference signals follow the Rayleigh distribution, i.e., $|g_k|^2 \sim \text{Rayleigh}\left(\eta_k\right)$, which is practical and widely considered in many works [31], [32]. Note that the large scale fading of the interference signal is considered in the mean value of g_k. We then use the $\alpha - \mu$ distribution to model the small-scale fading, which is a general fading model that includes several important other distributions, such as the Weibull, One-Sided Gaussian, Rayleigh, and Nakagami. The probability density function (PDF) and the cumulative distribution function (CDF) expressions of a squared $\alpha - \mu$ random variable $|h_{jk}|^2$ are given by [33]:

$$f_{|h_{jk}|^2}(x) = \frac{\alpha x^{\frac{\alpha\mu}{2}-1}}{2\beta^{\frac{\alpha\mu}{2}} \Gamma(\mu)} \exp\left(-\left(\frac{x}{\beta}\right)^{\frac{\alpha}{2}}\right), \qquad (3)$$

and

$$F_{|h_{jk}|^2}(x) = \frac{\gamma\left(\mu, x^{\frac{\alpha}{2}} \beta^{-\frac{\alpha}{2}}\right)}{\Gamma(\mu)}, \qquad (4)$$

respectively, where $\Gamma(\cdot)$ is the gamma function [34, eq. (8.310.1)], $\beta = \frac{\tilde{\Upsilon}\Gamma(\mu)}{\Gamma\left(\mu+\frac{2}{\alpha}\right)}$, and $\gamma(\cdot)$ is the incomplete gamma function [34, eq. (8.35)].
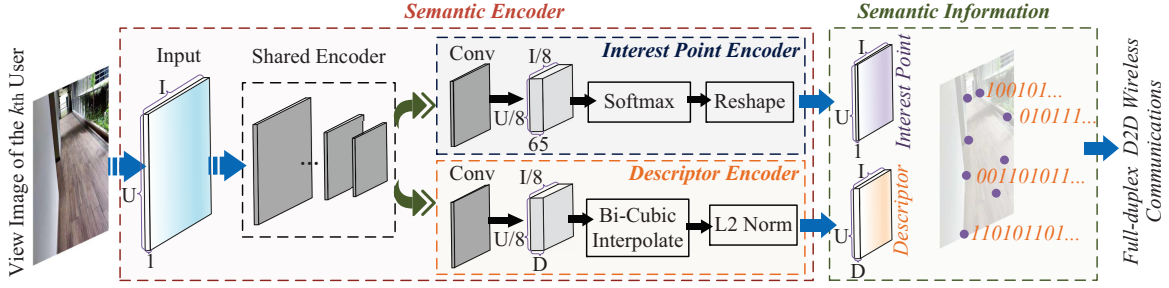
Fig. 4. The structure of the semantic encoder. The input is the user's view image, and the output is the detected interest points and descriptors.

The received signal-to-interference-plus-noise Ratio (SINR) of the kth user can be expressed as

$$\gamma_k = \frac{P_j D_{jk}^{-\beta_k} |h_{jk}|^2}{P_I \sum\limits_{i=1}^{N} |g_k|^2 + v_k P_k \sigma_S^2 + \sigma_N^2}. \quad (5)$$

Simply, the SINR received by the jth user can be obtained by interchanging j and k in (5). Note that the value of SINR affects the BEP and achievable rate in the wireless semantic information transmission. In full-duplex communications, the higher the transmit power of one user, the larger the value of SINR of the received signal of the other user. Considering that the total energy of the user's MR HMD is limited, incentives can be used to encourage users to share information, which is discussed in Section V-A.

IV. SEMANTIC MATCHING AND CONTRACT MODELLING

In this section, we propose the semantic encoder design scheme according to SuperPoint [24] and the semantic matching scheme according to SuperGlue [25], using the received semantic information to perform view images matching.

A. Self-Supervised Semantic Encoding

The definition of semantic information is typically task-relevant. For source messages in image modality, semantic information can be in the form of knowledge graphs [35], semantic segmentation results [36], or features [37]. In our proposed D2D free-space information sharing framework, the semantic information extracted from one user's view image needs to be used to help a second user determine the spatial correspondence between two view images.

As we discussed in Section II-B, convolutional neural network (CNN) has been widely used in interest point detection and description. Here, we utilize the self-supervised Super-Point [24] architecture as the semantic encoder to produce interest point detection accompanied by fixed length descriptors in a single forward pass. Specifically, as shown in Fig. 4, the full-sized view image of the kth user is sent to a shared CNN to reduce the dimensionality of the input view image. The output is then fed to two separate encoders to obtain the interest points and descriptors, respectively. We next present the introduction to each component and the design of the loss function.

- *Shared CNN Encoder:* To reduce the dimensionality of the input view image, the shared encoder uses the VGG-style [38] architecture. The encoder consists of convolutional layers, spatial down-sampling via pooling and non-linear activation functions [24]. The encoder maps an input image to an intermediate tensor with smaller spatial dimension and greater channel depth.
- *Interest Point Encoder:* The interest point encoder in the semantic encoder can be designed with an explicit decoder to reduce the computation of the model [39]. After a channel-wise softmax layer, the dustbin dimension is removed and the reshape is performed.
- *Descriptor Encoder:* A model similar to UCN [40] is used in the descriptor encoder to first output a semi-dense grid of descriptors. The decoder then performs bicubic interpolation of the descriptor. The activation is $L2$-normalized to be unit length, as shown in Fig. 4.
- *Loss Function Design:* The loss function of the semantic encoder can be written as the sum of the loss functions of the two encoders, i.e., interest point and descriptor encoders. According to the SuperPoint [24], pairs of synthetically warped images can be used to train the network.

After the network is trained, the required interest points and descriptors can be quickly obtained by inputting the user's view image. It has been shown that SuperPoint-based network architecture can support real-time interest points and descriptors extraction [24].

The extracted interest points and descriptors are received by other users via D2D full-duplex wireless transmission and then used. The performance metrics in wireless transmission are discussed in Section V. We first discuss the semantic information matching problem after successful reception in the following.

B. Semantic Information Matching

In the full-duplex system under our consideration, the semantic encoders discussed in the previous section should be deployed in each MR HMD, as shown in Fig. 3. After other users receive the interest points and descriptors, semantic information extraction should also be performed on the user's own view image. Then, the semantic information matching is performed among the extracted interest points and descriptors. Here, we use SuperGlue [25] as a semantic matching network
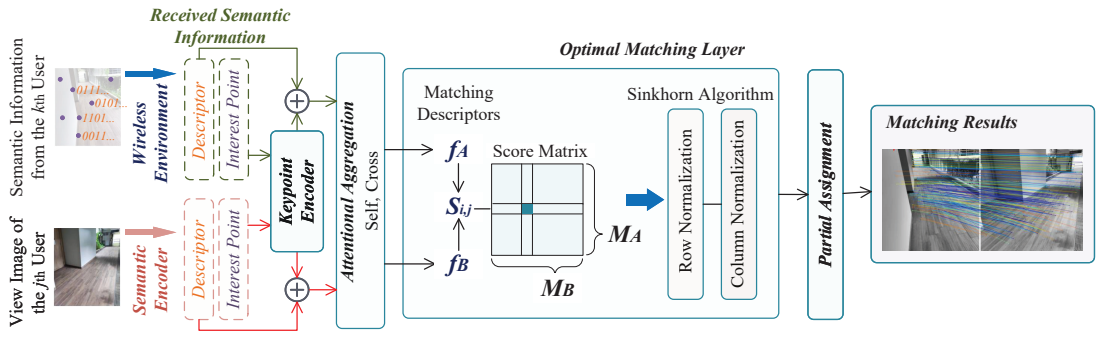
Fig. 5. The structure of the semantic matching. The input is the received semantic information and the jth user's semantic encoding results, and the output is the matching results.

architecture. Note that a user may share its semantic information to multiple users in the form of D2D full-duplex wireless communication, each user is independent when matching semantic information. Therefore, in the following discussion we focus on the matching between the two view images.

Here, the semantic information of one image, i.e., interest point and descriptors, obtained by the semantic encoder can be regarded as the local features. We consider that images A and B have M_A and M_B local features, respectively. According to the SuperGlue [25], for the integration into downstream tasks and better interpretability, each possible correspondence should have a confidence value. We consequently define a partial soft assignment matrix $\mathbf{P} \in [0, 1]^{M_A \times M_B}$ as $\mathbf{P}\mathbf{1}_{M_B} \leqslant \mathbf{1}_{M_A}$, and $\mathbf{P}^{\text{T}}\mathbf{1}_{M_A} \leqslant \mathbf{1}_{M_B}$. The goal is to design a neural network that predicts the assignment $\mathbf{P}$ from two sets of local features. In the following, we introduce the main components and the design of the loss function.

- *Attentional Graph Neural Network:* To enhance the uniqueness of points of interest and descriptors, we can consider the relationship between a certain pair of points of interest and descriptors and other pairs, such as the ones that are salient, self-similar, statistically co-occurring, or adjacent [41]. Also, notice that when humans are asked to match a given pair blurred key points, the humans look back and forth on both images [42]. This implies that an iterative process can focus the attention on a specific correct location. Thus, the first major block of SuperGlue is designed as an Attentional Graph Neural Network (AGNN) [25]. For given initial local features, the AGNN computes matching descriptors by allowing features interact with other features. We embed the keypoint position into a high dimensional vector with a Multilayer Perception (MLP), which enables the graph network to later reason about both appearance and position jointly, especially when combined with attention [43].
- *Optimal Matching Layer:* The optimal matching layer is the second major block of SuperGlue. It is used to produce a partial assignment matrix. As in the standard graph matching formulation, the assignment $\mathbf{P}$ can be obtained by computing a score matrix $\mathbf{S} \in \mathbb{R}^{M_A \times M_B}$ for all possible matches and maximizing the total score $\sum_{i,j} \mathbf{S}_{i,j} \mathbf{P}_{i,j}$. This is equivalent to solving a linear

assignment problem. The optimal matching layer creates an $M_A \times M_B$ score matrix, augments it with dustbins, and then finds the optimal partial assignment by using the Sinkhorn algorithm [44]. After T iterations, we drop the dustbins and recover $\mathbf{P} = \bar{\mathbf{P}}_{1:M_A, 1:M_B}$.
- *Loss Function Design:* Both the AGNN and the optimal matching layer are differentiable, which allows back propagation from matches to visual descriptors. Note that SuperGlue is trained in a supervised manner from ground truth matches [25]. Given these labels, we minimize the negative log-likelihood of the assignment $\bar{\mathbf{P}}$. This supervision aims at simultaneously maximizing the precision and the recall of the matching. After training, the model can be used in the user's MR HMDs to match semantic information, after receiving semantic features from the transmitter and extracting its own interest points and descriptors from the view image.

C. Contract Modelling

We use a contract as the incentive to encourage users to share the semantic information with each other. The payment plan and the utilities of the SIP and SIR are formulated respectively.

1) Payment Plan: To promote MR users' participation in the semantic information sharing, an appropriate payment plan is required that allows both SIP and SIR benefit from the cooperation. To this end, we propose a contract theoretic payment plan, in which the SIP receives the compensation from the SIR according to quality of the shared semantic information (QoS). Thus, the resulting revenue function of the InP can be expressed as

$$I_{\text{SIP}} = c_q Q_s + c_f, \tag{6}$$

where c_f represents the payment made by the SIR to the SIP for the computation resource consumption in semantic encoding, the parameter c_q denotes the fee charged for a unit QoS value, and Q_s is the quantified value of the QoS of the SIR.

While the proposed semantic information extraction and matching schemes in Sections IV-A and IV-B demonstrate efficiency and feasibility, the semantic matching outcomes are subject to the wireless transmission process. The achievable rate impacts the latency of the information sharing, while the

BEP affects the accuracy of the received semantic information. Hence, we define the QoS as

$$Q_s(P_k) = M_k \mathcal{T}(R_k) \mathcal{T}(1 - E_k), \tag{7}$$

where $M_k \in [0, 1]$ indicate the impact of the semantic extraction and matching algorithm on QoS[2], R_k is the achievable rate, E_k is the BEP, and the function $\mathcal{T}(\cdot)$ is used to eliminate the effect of the magnitudes [45], which is defined as

$$\mathcal{T}(t) = \frac{t - t_{\min}}{t_{\max} - t_{\min}}, \tag{8}$$

where $t_{\min}$ is the minimal threshold, $t_{\max}$ is the maximal value that SIP can provide.

2) Utility of The Semantic Information Provider: The utility of the SIP can be obtained as

$$U_{\text{SIP}} = I_{\text{SIP}} - c_p P_k = c_q Q_s - c_p P_k + c_f, \tag{9}$$

where P_k is the transmit power of the SIP and c_p represents the unit cost of P_k.

3) Utility of The Semantic Information Receiver: As we discussed in Section III-A, SIR can match spatial locations with the SIP using the received semantic information. Therefore, the higher the Q_s, the more accurate the results achieved by SIR through matching, and the more computation resources can be saved. We use the parameter c_s to measure the utility gain per unit Q_s boost to SIR. The utility of the SIR can be then expressed as

$$U_{\text{SIR}} = c_s Q_s - I_{\text{SIP}} = (c_s - c_q) Q_s - c_f. \tag{10}$$

4) Contract Modelling: The contract provided by the SIR includes two items, i.e., $\{c_q, c_f\}$. To design the optimal contract, we formulate the SIR's utility maximization problem while providing the SIP with the necessary incentives to agree on the contract. The optimization problem can be expressed as [46]

$$\max_{c_q, c_f, P_k} \quad U_{\text{SIR}}(c_q, c_f, P_k)$$
$$\text{s.t.} \quad \begin{cases} P_k{}^* \in \arg\max_{P_k} U_{\text{SIP}}(P_k, c_q, c_f), \\ U_{\text{SIP}}(P_k{}^*, c_q, c_f) \geq U_{\text{th}}^{\text{SIP}}, \end{cases} \tag{11}$$

where the first constraint is the IC constraint [47], i.e., $P_k{}^*$ is set to maximize its own utility. The second is the IR constraint [47] with a utility threshold $U_{\text{th}}^{\text{SIP}}$.

We first consider the IC constraint. The closed-form expression of QoS can be derived in Section V. For a given contract $\{c_q, c_f\}$, we can solve the IC constraint to obtain the optimal power and corresponding Q_s^*. Accordingly, we substitute the IR constraint with the optimal power and simplify the SIR maximization problem. Therefore, the optimal contract design, $\{c_q{}^*, c_f{}^*\}$, is modeled as a complex decision-making problem. Whereas conventional mathematical techniques may encounter tractability challenges in addressing a given problem, DRL-based methods might offer a viable alternative.

However, the optimal contract design for a wireless communication system is impacted not only by user-specific factors

such as price per unit of power, but also by the intricate wireless milieu, including co-channel interference signal power, the count of interference paths, and different parameters associated with small-scale fading as discussed in Section III-B. As a result, the DRL-based algorithms may struggle to converge to the optimal solution or achieve suboptimal performance due to the high dimensionality of the state. To address this challenge, the choice of DRL algorithms can be crucial to improve the effectiveness. Proximal Policy Optimization (PPO) and Soft Actor-Critic (SAC) are two popular DRL algorithms that have shown promising results in high-dimensional state problems. PPO is an on-policy algorithm that optimizes the policy by iteratively updating the policy using a clipped surrogate objective. It prevents large policy updates and promotes smooth policy changes. On the other hand, SAC is an off-policy algorithm that learns a stochastic policy to maximize both the expected cumulative reward and the entropy of the policy. SAC is known for its ability to handle continuous action spaces and can achieve state-of-the-art performance in a variety of tasks.

Therefore, we solve the optimal contract design problem, i.e., (11), using two DRL algorithms, i.e., PPO and SAC. Moreover, to tackle the challenge of addressing high-dimensional state spaces using DRL algorithms, we propose a novel AI-generated contract method based on diffusion models in Section V-A. We then evaluate and compare the performance of our proposed method with that of the DRL schemes in Section VI-B.

V. AI-GENERATED CONTRACT AND PERFORMANCE ANALYSIS

In this section, we proposed an AI-generated contract method. Then, we derive the PDF expression of the SINR in the D2D full-duplex communication system. The closed-form achievable rate and BEP are also derived.

A. AI-Generated Contract

1) Diffusion Model: Diffusion-based generative models pose the data-generating process as an iterative denoising procedure. This denoising is the opposite of a forward diffusion process, which gradually corrupts the data's structure by introducing noise. Specifically, diffusion models are latent variable models of the form

$$p_\theta(\mathbf{x}_0) := \int p_\theta(\mathbf{x}_{0:T}) d\mathbf{x}_{1:T}, \tag{12}$$

where $\mathbf{x}_1, \ldots, \mathbf{x}_T$ are latents of the same dimensionality as the data $\mathbf{x}_0 \sim p(\mathbf{x}_0)$. The joint distribution in (12), i.e., $p_\theta(\mathbf{x}_{0:T})$, is called the *reverse diffusion*, which is defined as a Markov chain with learned Gaussian transitions starting at $p(\mathbf{x}_T) = \mathcal{N}(\mathbf{x}_T; \mathbf{0}, \mathbf{I})$ as

$$p_\theta(\mathbf{x}_{0:T}) := p(\mathbf{x}_T) \prod_{t=1}^{T} p_\theta(\mathbf{x}_{t-1} \mid \mathbf{x}_t), \tag{13}$$

where

$$p_\theta(\mathbf{x}_{t-1} \mid \mathbf{x}_t) := \mathcal{N}(\mathbf{x}_{t-1}; \mu_\theta(\mathbf{x}_t, t), \mathbf{\Sigma}_\theta(\mathbf{x}_t, t)). \tag{14}$$

---

[2]Because M_k is only decided by the chosen semantic encoding and matching algorithms, we set $M_k = 1$ without loss of generality.
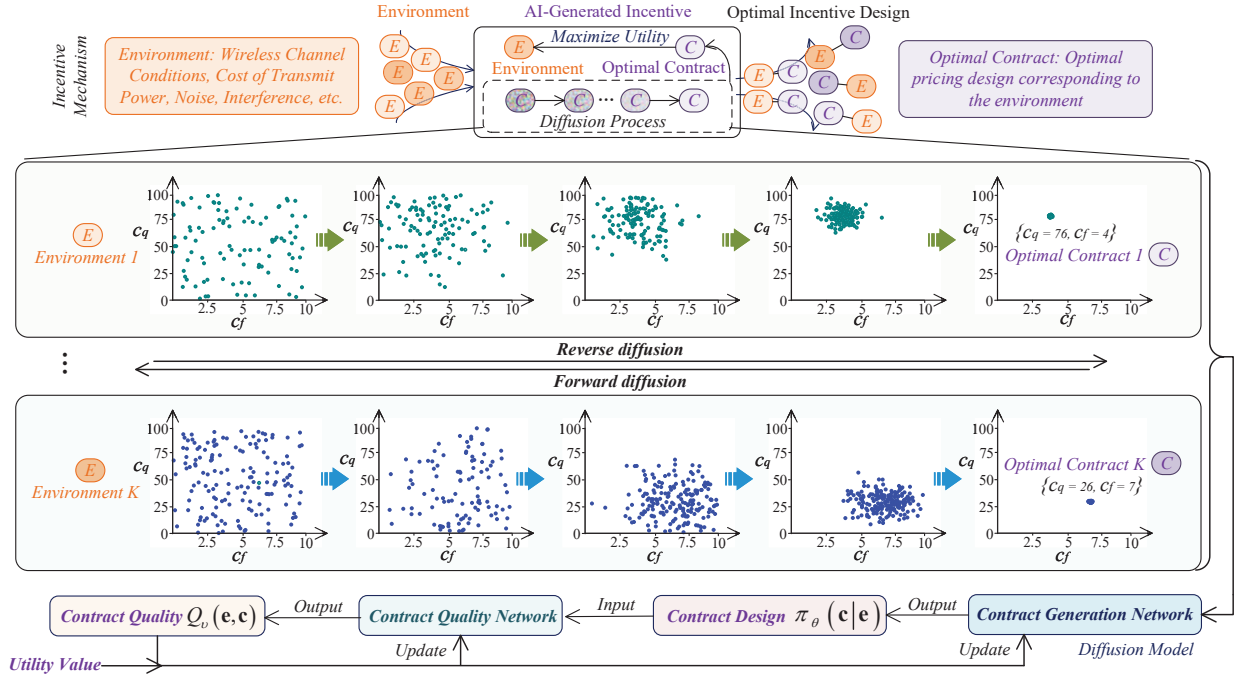
Fig. 6. Diffusion Model for incentive design. Diffusion Model for incentive design. For any given environment, the contract is first randomly generated as the Gaussian noise. After the multi-step denoising through the diffusion model, the output is the contract design that maximizes the optimization objective.

A *forward diffusion* chain gradually adds noise to the data as a Markov chain according to a variance schedule $\beta_1, \ldots, \beta_T$ as

$$q\left(\mathbf{x}_{1:T} \mid \mathbf{x}_0\right) := \prod_{t=1}^{T} q\left(\mathbf{x}_t \mid \mathbf{x}_{t-1}\right), \qquad (15)$$

where

$$q\left(\mathbf{x}_t \mid \mathbf{x}_{t-1}\right) := \mathcal{N}\left(\mathbf{x}_t; \sqrt{1-\beta_t}\mathbf{x}_{t-1}, \beta_t \mathbf{I}\right). \qquad (16)$$

After training, sampling from the diffusion model consists of sampling $\boldsymbol{x} \sim p(x_T)$ and running the reverse diffusion chain to go from $t = T$ to $t = 0$. Diffusion models can be straightforwardly extended to conditional models by conditioning $p_\theta(\mathbf{x}_{t-1} \mid \mathbf{x}_t, c)$.

2) AI-Generated Contract: We explain how to apply a conditional diffusion model to generate the contract design, i.e., $\{c_q, c_f\}$ in (11). In contrast to the conventional utilization of back propagation algorithms in neural networks or DRL techniques that directly optimize model parameters, diffusion models aim to enhance contract design by iterative denoising the initial distribution, leading to generating a utility function of greater efficacy.

As we discussed in Section IV-C4, the optimal contract is related to multiple variables that are unknown to the SIR. We use the vector $\boldsymbol{e}$ to denote the environment, i.e., the set of all variables, that affects the optimal contract design as

$$\boldsymbol{e} = \left\{c_s, c_p, D_{jk}, \beta_k, \alpha, \mu, \sigma_N^2, \sigma_S^2, \upsilon_k, P_I, \eta_k, N, P_j\right\}. \qquad (17)$$

We denote the contract to be designed by the SIR in the given environment as $\boldsymbol{c} = \{c_q, c_f\}$. We call the diffusion model network that maps environment states to contract designs as the *contract design policy*, i.e., $\pi_\theta(\boldsymbol{c} \mid \boldsymbol{e})$ with parameters

θ. The goal of $\pi_\theta(\boldsymbol{c} \mid \boldsymbol{e})$ is to output deterministic contract design that maximizes the expected cumulative reward over a sequence of time steps. We represent the *contract design policy* via the reverse process of a conditional diffusion model as

$$\pi_\theta(\boldsymbol{c} \mid \boldsymbol{e}) = p_\theta\left(\boldsymbol{c}^{0:N} \mid \boldsymbol{e}\right) = \mathcal{N}\left(\boldsymbol{c}^N; \mathbf{0}, \boldsymbol{I}\right) \prod_{i=1}^{N} p_\theta\left(\boldsymbol{c}^{i-1} \mid \boldsymbol{c}^i, \boldsymbol{e}\right). \qquad (18)$$

As shown in Fig. 6, the end sample of the reverse chain is the final chosen contract design. Here, $p_\theta\left(\boldsymbol{c}^{i-1} \mid \boldsymbol{c}^i, \boldsymbol{e}\right)$ can be modeled as a Gaussian distribution $\mathcal{N}\left(\mathbf{c}^{i-1}; \mu_\theta\left(\mathbf{c}^i, \mathbf{e}, i\right), \boldsymbol{\Sigma}_\theta\left(\mathbf{c}^i, \mathbf{e}, i\right)\right)$. According to [48], $p_\theta\left(\boldsymbol{c}^{i-1} \mid \boldsymbol{c}^i, \boldsymbol{e}\right)$ can be modeled as a noise prediction model with the covariance matrix fixed as

$$\boldsymbol{\Sigma}_\theta\left(\boldsymbol{c}^i, \boldsymbol{e}, i\right) = \beta_i \boldsymbol{I}, \qquad (19)$$

and mean constructed as

$$\mu_\theta\left(\mathbf{c}^i, \mathbf{e}, i\right) = \frac{1}{\sqrt{\alpha_i}}\left(\mathbf{c}^i - \frac{\beta_i}{\sqrt{1-\bar{\alpha}_i}}\boldsymbol{\varepsilon}_\theta\left(\mathbf{c}^i, \mathbf{e}, i\right)\right). \qquad (20)$$

We first sample $\boldsymbol{c}^N \sim \mathcal{N}(\mathbf{0}, \mathbf{I})$ and then from the reverse diffusion chain parameterized by θ as

$$\mathbf{c}^{i-1} \mid \mathbf{c}^i = \frac{\mathbf{c}^i}{\sqrt{\alpha_i}} - \frac{\beta_i}{\sqrt{\alpha_i\left(1-\bar{\alpha}_i\right)}}\boldsymbol{\varepsilon}_\theta\left(\mathbf{c}^i, \mathbf{e}, i\right) + \sqrt{\beta_i}\boldsymbol{\varepsilon}. \qquad (21)$$

Therefore, the task of training the *contract design policy* π_θ in complex and high-dimensional environments $\boldsymbol{e}$ is effectively transferred to training a *contract generation network* $\boldsymbol{\varepsilon}_\theta$. Following DDPM [48], when $i = 1$, $\boldsymbol{\varepsilon}$ is set as 0 to improve the sampling quality. Furthermore, to train the $\boldsymbol{\varepsilon}_\theta$, motivated by the Q-function in DRL, we define the *contract quality network* Q_υ that maps an environment-contract pair, i.e., $\{\boldsymbol{e}, \boldsymbol{c}\}$, to a value

representing the expected cumulative reward if an agent takes one contract design policy from the current state and follows the policy thereafter. Thus, the optimal *contract design policy* is the policy that maximizes the expected cumulative utility of the SIR, which can be obtained by

$$\pi = \arg\min_{\pi_\theta} \mathcal{L}(\theta) = -\mathbb{E}_{\mathbf{c}^0 \sim \pi_\theta}\left[Q_\upsilon\left(\mathbf{e}, \mathbf{c}^0\right)\right]. \quad (22)$$

The *contract quality network* is learned in a conventional way, minimizing the Bellman operator with the double Q-learning technique [49]. Two networks, namely Q_{υ_1} and Q_{υ_2}, along with target networks, namely $Q_{\upsilon'_1}$, $Q_{\upsilon'_2}$ and $\pi_{\theta'}$, are constructed. We then optimize υ_i for $i = \{1, 2\}$ by minimizing the objective

$$\mathbb{E}_{\mathbf{c}^0_{t+1} \sim \pi_{\theta'}}\left[\left\|\left(r(\mathbf{e}, \mathbf{c}_t) + \gamma \min_{i=1,2} Q_{\upsilon'_i}(\mathbf{e}, \mathbf{c}^0_{t+1})\right) - Q_{\upsilon_i}(\mathbf{e}, \mathbf{c}_t)\right\|^2\right]. \quad (23)$$

Specifically, our AI-generated contract algorithm involves generating a contract design using the denoising technique, followed by adding exploration noise to the contract design and executing it to gain the exploring experience. The algorithm for AI-generated contract is shown in **Algorithm 1**. By utilizing **Algorithm 1**, we can obtain the optimal contract based on the wireless system environment vector. The performance of the proposed AI-generated contract algorithm is compared with conventional DRL algorithms in Section VI.

Remark 1. *Our proposed diffusion model-based AI-generated contract algorithm learns experience from the environment in an exploratory manner and achieves the optimal solution using the diffusion model. By gradually adjusting the output, the diffusion model is more robust and effective than the neural network model that directly outputs the solution. We believe that our proposed innovative algorithm can be easily extended to various problems in wireless communication networks, such as resource allocation, game theoretic incentive mechanism design, and reinforcement learning and federal learning algorithm optimization.*

In the following, we further analyze the performance of the full-duplex wireless system and provide more insights.

B. Performance Analysis

After obtaining the semantic information according to the scheme in Section IV-A, the user transmits the semantic information to other users in the form of D2D full-duplex communications with the contract incentive. Nevertheless, the wireless medium is subject to various impairments such as small-scale fading, self-interference, co-channel interference and noise, which inevitably degrade the achievable rate and BEP. To obtain the closed-form expressions with parameters capable of describing the above phenomenon in the semantic information D2D full-duplex transmission, we first perform the following performance analysis.

1) PDF and CDF expressions: To obtain the closed-form expressions of the achievable rate and the BEP of the D2D full-duplex communication links, we first derive the PDF expression of the SINR.

Algorithm 1 The Algorithm for AI-Generated Contract

Training Phase:
1: Input hyper-parameters: diffusion step N, batch size N_b, discount factor γ, soft target update parameter τ, exploration noise ϵ
2: ## *Initialize NN*
3: Initialize replay buffer R, contract generation network $\boldsymbol{\varepsilon}_\theta$ with weights θ, contract quality network Q_υ with weights υ, target contract generation network $\boldsymbol{\varepsilon}'_{\theta'}$ with weights θ', target contract quality network $Q'_{\upsilon'}$ with weights υ'
4: ## *Learning*
5: **for** Episode = 1 **to** Max_episode **do**
6:    Initialize a random process $\mathcal{N}$ for contract design exploration
7:    **for** Step = 1 **to** Max_step **do**
8:       Observe the current environment $\boldsymbol{e}_t$
9:       **Set $\boldsymbol{c}^N_t$ as Gaussian noise. Generate contract design $\boldsymbol{c}^0_t$ by denoising $\boldsymbol{c}^N_t$ using $\boldsymbol{\varepsilon}_\theta$ according to** (21)
10:       Add the exploration noise ϵ to $\boldsymbol{c}^0_t$
11:       Execute contract design $\boldsymbol{c}^0_t$ and observe reward U_{SIR} that is defined as (10)
12:       Store the record $(\boldsymbol{e}_t, \boldsymbol{c}^0_t, r_t)$ in replay buffer R
13:       Sample a random minibatch of N_b records $(\boldsymbol{e}_i, \boldsymbol{c}_i, r_i)$ from R
14:       Set $y_i = r_i + \gamma Q'_{\upsilon'}\left(\boldsymbol{e}_i, \boldsymbol{c}'^0_t\right)$, where $\boldsymbol{c}'^0_t$ is obtained using $\boldsymbol{\varepsilon}'_{\theta'}$
15:       Update the *contract quality network* by minimizing the loss:
16:         $\mathcal{L} = \frac{1}{N_b}\sum_i (y_i - Q_\upsilon(\boldsymbol{e}_i, \boldsymbol{c}_i))^2$
17:       Update the *contract generation network* by computing the policy gradient:
18:         $\nabla_\theta \boldsymbol{\varepsilon}_\theta \approx \frac{1}{N_b}\sum_i \nabla_{\boldsymbol{c}^0} Q_\upsilon(\boldsymbol{e}, \boldsymbol{c}^0)\,|_{\boldsymbol{e}=\boldsymbol{e}_i} \nabla_\theta \boldsymbol{\varepsilon}_\theta |\boldsymbol{e}_i$
19:       Update the target networks:
20:         $\theta' \leftarrow \tau\theta + (1-\tau)\theta'$,
21:         $\upsilon' \leftarrow \tau\upsilon + (1-\tau)\upsilon'$
22:    **end for**
23: **end for**
24: **return** The trained *contract generation network* $\boldsymbol{\varepsilon}_\theta$

Inference Phase:
1: Input the environment vector $\boldsymbol{e}$
2: Generate the optimal contract design $\boldsymbol{c}^0$ by denoising Gaussian noise using $\boldsymbol{\varepsilon}_\theta$ according to (21)
3: **return** The optimal contract design $\boldsymbol{c}^0$

Lemma 1. *The closed-form PDF and CDF expressions of the SINR can be derived as*

$$f_{\gamma_k}(x) = \frac{\alpha x^{-1}}{2\Gamma(N)\Gamma(\mu)}$$
$$\times H^{0,0:0,1;1,1}_{1,0:1,1;1,1}\left(\begin{array}{c}\left(\frac{\varphi x D^{\beta_k}_{jk}}{\beta P_j}\right)^{\frac{-\alpha}{2}} \\ \frac{\varphi}{\eta_k P_I}\end{array}\middle| \begin{array}{c}(0; -\frac{\alpha}{2}, 1){:}(1-\mu, 1);(1,1) \\ - : \left(1, \frac{\alpha}{2}\right);(N, 1)\end{array}\right),$$
$$(24)$$

and

$$F_{\gamma_k}(x) = \frac{\alpha}{2\Gamma(N)\Gamma(\mu)}$$
$$\times H^{0,0:1,1;1,1}_{1,0:1,2;1,1}\left(\begin{array}{c}\left(\frac{\beta P_j}{\varphi x D^{\beta_k}_{jk}}\right)^{\frac{\alpha}{2}} \\ \frac{\varphi}{\eta_k P_I}\end{array}\middle| \begin{array}{c}(0; -\frac{\alpha}{2}, 1){:}(1-\mu, 1)\left(1, \frac{\alpha}{2}\right);(1,1) \\ - : \left(0, \frac{\alpha}{2}\right)\left(1, \frac{\alpha}{2}\right);(N, 1)\end{array}\right),$$
$$(25)$$

where $H^{::}_{::}(\cdot|\cdot)$ is the Multivariate Fox's H-function [50, eq. (A-1)].

Proof: Please refer to Appendix A. ∎

2) Approximation Analysis: To simplify the mathematical tractability of the derived PDF and CDF expressions, we further study a practical special scenario, namely, the interference-limited case. Specifically, we consider that the noise is negligible, i.e., $\sigma_N^2 = 0$, and the user's HMD is equipped with an efficient self-interference cancellation technique, i.e., $\upsilon = 0$. Then, we can re-write the SNR as

$$\gamma_{k'} = \frac{P_j D_{jk}^{-\beta_k} |h_{jk}|^2}{P_I \sum\limits_{i=1}^{N} |g_k|^2}. \tag{26}$$

The simplified PDF and CDF expressions can be derived.

Lemma 2. *We derive the approximated PDF and CDF expressions when $\sigma_N^2 = 0$ and $\upsilon = 0$ as*

$$f_{\gamma_k}(x) = \frac{\alpha x^{\frac{\alpha\mu}{2}-1}(\eta_k P_I)^{\frac{\alpha\mu}{2}}}{2\left(P_j D_{jk}^{-\beta_k}\beta\right)^{\frac{\alpha\mu}{2}}\Gamma(N)\Gamma(\mu)}$$
$$\times H_{1,1}^{1,1}\left(\left(\frac{\beta P_j D_{jk}^{-\beta_k}}{\eta_k P_I x}\right)^{\frac{\alpha}{2}}\left|\begin{array}{c}(1;1)\\\left(\frac{\alpha\mu}{2}+N;\frac{\alpha}{2}\right)\end{array}\right.\right), \tag{27}$$

and

$$F_{\gamma_k}(x) = \frac{\alpha(y\eta_k P_I)^{\frac{\alpha\mu}{2}}}{2\left(P_j D_{jk}^{-\beta_k}\beta\right)^{\frac{\alpha\mu}{2}}\Gamma(N)\Gamma(\mu)}$$
$$\times H_{2,2}^{2,1}\left(\left(\frac{\beta P_j D_{jk}^{-\beta_k}}{\eta_k P_I y}\right)^{\frac{\alpha}{2}}\left|\begin{array}{c}(0;1)\left(\frac{\alpha\mu}{2}+1;\frac{\alpha}{2}\right)\\\left(\frac{\alpha\mu}{2}+N;\frac{\alpha}{2}\right)\left(\frac{\alpha\mu}{2};\frac{\alpha}{2}\right)\end{array}\right.\right). \tag{28}$$

Proof: Please refer to Appendix B. ∎

With the aid of Lemma 2, the performance analysis of a full-duplex system operating in an interference-limited scenario can be simplified. In particular, the outage probability (OP) can be expressed as the probability that the received SNR falls below a given outage threshold γ^{th}, which can be mathematically represented as $P_O = \mathbb{P}\left(\gamma_k < \gamma^{\text{th}}\right) = F\gamma_k\left(\gamma^{\text{th}}\right)$. To evaluate the OP, we can utilize (28). Additionally, when the transmit power of the jth user is high, i.e., $P_j \to \infty$, the OP can be further simplified by calculating the residue at the nearest pole to the Mellin-Barnes integral contour of the Meijer's G-function [34]

$$P_O \approx \frac{(\gamma_{th}\eta_k P_I)^{\frac{\alpha\mu}{2}}}{\mu\left(P_j D_{jk}^{-\beta_k}\beta\right)^{\frac{\alpha\mu}{2}}\Gamma(N)\Gamma(\mu)}\Gamma\left(\frac{\alpha\mu}{2}+N\right). \tag{29}$$

Figure 7 shows the OP of the kth user versus the transmit power of the jth user under different transmit distance. As shown in the figure, the OP increases as the transmission distance increases. Moreover, in the high P_j region, our derived approximate expression yields the result close to that from the exact expression, thereby validating the accuracy of our approximate analysis.

3) Achievable Rate in Full-duplex Communications: The ergodic achievable rate (or Shannon capacity) for the trans-
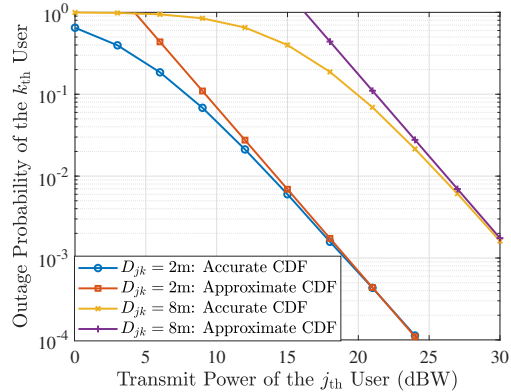

Fig. 7. The outage probability of the kth user versus the transmit power of the jth user under different transmit distance, with $\beta_k = 2$, $\alpha = 2$, $\mu = 2$, $P_k = 0$ dBW, $P_I = 1$ dBW, $\eta_k = 0.2$, $\upsilon_k = 0.2$, and $N = 2$.

mitter, which is known to be the maximum data rate that the channel can support (per Hz), is defined as

$$C_k = \int_0^\infty \log_2(1+x)f_{\gamma_k}(x)\mathrm{d}x. \tag{30}$$

Then, with the help of Lemma 1, the achievable rate can be obtained in the following theorem.

Theorem 1. *The achievable rate of the kth user, i.e., C_k, can be derived in closed-form as*

$$C_k = \frac{\Gamma^{-1}(\mu)\alpha}{\ln 4\Gamma(N)}$$
$$\times H_{1,0:3,3;1,1}^{0,0:1,3;1,1}\left(\left(\frac{\beta P_j}{\varphi D_{jk}^{\beta_k}}\right)^{\frac{\alpha}{2}}\left|\begin{array}{c}(0;-\frac{\alpha}{2},1):(1-\mu,1)(1,\frac{\alpha}{2})(1,\frac{\alpha}{2});(1,1)\\-:(1,\frac{\alpha}{2})(0,\frac{\alpha}{2})(1,\frac{\alpha}{2});(N,1)\end{array}\right.\right). \tag{31}$$

Proof: Please refer to Appendix C ∎

4) Bit Error Probability in Full-duplex Communications: The average BEP for the kth user under a variety of modulation formats is given by [51]

$$E_k = \int_0^\infty \frac{\Gamma(\tau_2,\tau_1\gamma)}{2\Gamma(\tau_2)}f_{\gamma_k}(\gamma)\,d\gamma, \tag{32}$$

where $\Gamma(\cdot,\cdot)$ is the upper incomplete Gamma function [34, eq. (8.350.2)], $\Gamma(\tau_2,\tau_1\gamma)/2\Gamma(\tau_2)$ is the conditional bit-error probability, τ_1 and τ_2 are modulation-specific parameters that represents various modulation/detection combinations. Specifically, $\{\tau_1 = 1, \tau_2 = 0.5\}$ is antipodal coherent binary phase-shift keying (BPSK), $\{\tau_1 = 0.5, \tau_2 = 0.5\}$ denote orthogonal coherent binary frequency-shift keying (BFSK), $\{\tau_1 = 0.5, \tau_2 = 1\}$ is orthogonal non-coherent BFSK, and $\{\tau_1 = 1, \tau_2 = 1\}$ denote antipodal differentially coherent BPSK (DPSK).

Theorem 2. *The closed-form expression of the BEP of the kth*

user, i.e., E_k, is derived as

$$E_k = \frac{\alpha \tau_1^{\frac{\alpha}{2}t_1} \Gamma^{-1}(\tau_2)}{4\Gamma(N)\Gamma(\mu)}$$

$$\times H_{1,1:2,2;1,1}^{0,1:1,1;1,1} \left(\left. \begin{pmatrix} \left(\frac{\beta P_j}{\varphi D_{jk}^{\beta_k}}\right)^{\frac{\alpha}{2}} \\ \frac{\varphi}{\eta_k P_I} \end{pmatrix} \right| \begin{matrix} (1;-\frac{\alpha}{2},1):(1-\mu,1)\,(1,\frac{\alpha}{2});(1,1) \\ (1;\frac{\alpha}{2},-1):(0,\frac{\alpha}{2})\,(1,\frac{\alpha}{2});(N,1) \end{matrix} \right).$$

$$(33)$$

Proof: Please refer to Appendix D ∎

Remark 2. *The above derived performance indicator expressions contain the important channel parameters in a D2D full-duplex wireless communications system. Specifically, parameters that can respond to large-scale fading, small-scale fading, self-interference in duplex communications, and co-channel interference at arbitrary multipath are all included in (31) and (33). Detailed discussion is given in Section VI-C. Furthermore, the generalization of the small-scale fading model, i.e., α-μ fading channel model, allows us to use the derived performance metrics in the analysis of many systems with various kinds of fading conditions.*

Thus, we complete all the processes of the framework. Specifically, we use the semantic encoder in Section IV-A to extract interest point and descriptors. The computation task performed at the kth user could be the free-space information detection, which can be obtained by using the state-of-art anomaly detection approach named JSR-Net [28]. To motivate the semantic information sharing, we propose a contract theoretic mechanism to maximize the utility of SIR while ensuring that the utility of SIP is larger than the threshold of participation in sharing. In Section V-A, we propose the AI-generated contract algorithm based on the diffusion model to solve for the optimal contract design. For the D2D full-duplex wireless transmission, the performance analysis is comprehensively given in Section V-B. After SIRs receive the free-space information, interest points, and descriptors, the semantic matching scheme can be used to help the users obtain the free-space information in their own view images by matching instead of performing computation tasks again.

VI. NUMERICAL RESULTS

According to our core contributions, this section aims to answer the following research questions via experiments:

Q1) Can the proposed full-duplex semantic communication framework realize information sharing among users effectively?

Q2) On the basis of **Q1**, can the proposed incentive mechanism further boost the performance of information sharing, i.e., the utility of the SIR?

Q3) How do wireless channel and self-interference affect semantic information transmission during full-duplex D2D communication?

The experimental platform for running our proposed algorithms is built on a generic Ubuntu 20.04 system with an AMD Ryzen Threadripper PRO 3975WX 32-Cores CPU and an NVIDIA RTX A5000 GPU. In each Monte Carlo simulation,

we generated 10^6 random realizations of the channel to ensure statistical significance.

A. Effectiveness of semantic communication framework (for **Q1**)

First, we verify the effectiveness of the proposed D2D full-duplex semantic communications framework, and the results are shown in Fig. 8. As can be seen from the experimental results, firstly, according to the interest points, descriptors, and free-space information transmitted by the kth user, the jth user can effectively compute his own free-space information, as shown by the images in the first row. Compared with the conventional approach, i.e., the jth user computes the free-space information independently, this method consumes fewer resources since the jth user only needs to compute the spatial correspondence information between view images and conduct a corresponding spatial rotation to obtain his own free-space information. Secondly, the results demonstrate that as the BEP decreases, the free-space information computed by the jth user is more accurate, which finally generates a more accurate matching result, as presented by the images in the second row. Note that the values of BEP can be computed by using the environmental parameters and (33). This inspires us that the accuracy of semantic information during wireless transmission needs to be guaranteed in the free-space information sharing mechanism of D2D full-duplex communication systems.

It should be noted that due to the limitation of the viewing angle, some details, such as the corner marked by the black box in the jth user's view, cannot be obtained using the semantic information extracted from the view image of the kth user. However, this part of the information may be obtained through semantic information from users who have other different perspectives. Meanwhile, because full-duplex communication is taken into account here, the jth user would feed back the missing information to the kth user and other users, allowing the kth user to obtain more free-space information, even if there is a blind spot. Such real-time information updating mechanism is also an advantage of our proposed D2D framework.

B. Efficiency of the proposed incentive mechanism (for **Q2**)

Second, we present the comparison between our proposed AI-generated contract algorithm and two conventional DRL algorithms, i.e., SAC and PPO. The training process shown in Fig 9 (a) reveals that PPO requires more iteration steps to converge. Although SAC can stabilize at a higher reward faster, both the convergence rate and the final reward value are inferior to those of the AI-generated contract algorithm. We posit two reasons for this.

- Our algorithm achieves better sampling quality. Diffusion models can generate higher quality samples by fine-tuning multiple times. For example, we set the diffusion step to 10. Since each fine-tuning gradually adjusts the model's output, the effect of uncertain and noise can be reduced and the sampling accuracy is improved.
- Our algorithm possesses better long-term dependence processing capability. While conventional neural network
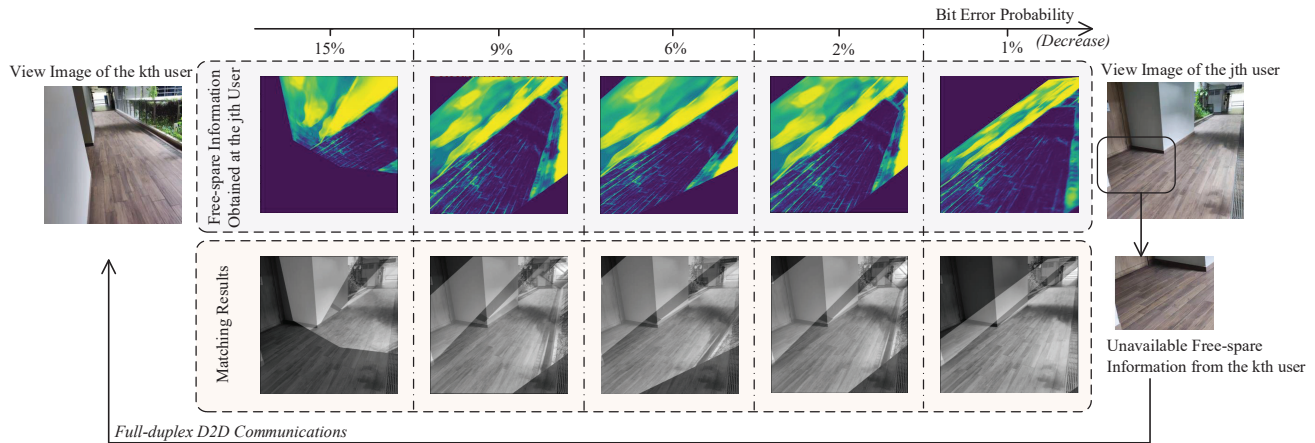
Fig. 8. The impact of different wireless transmission BEPs on our proposed full-duplex D2D free-space information sharing mechanism. The semantic encoder extracts 150 interest points and corresponding descriptors in the image as the semantic information.

generation models consider only the input at the current time step, the diffusion model allows the model to generate samples with more time steps by fine-tuning multiple times, thereby having better long-term dependence processing capability.

Furthermore, we compare the trained models' ability for optimal contract design in Fig 9 (b). For a given environment state, we observe that the AI-generated contract algorithm can provide a contract design that achieves the SIR utility value of 189.1, which is greater than the 185.9 achieved by the SAC and the 184.3 achieved by the PPO.

C. Influence of channel and self-interference (for Q3)

Third, we analyze the impact of wireless channels and self-interference on D2D full-duplex semantic communications. The effect of the jth user's (transmitter's) transmit power on the BEP of the kth user (receiver) is investigated in Fig. 10, during which the transmit power of kth user is fixed to 20 dBW. As the results show, as the transmit power of jth user increases from 0 to 20 dBW, the BEP of kth user decreases from about 10^{-1} to 10^{-5}. The clear reason is that since the increase in transmit power makes the SINR higher and thus reduces the BEP. Furthermore, the increase in interfering signal power raises the BEP, and the degree of BEP increase goes up as the transmit power increases. When the transmit power is 0 dBW, for example, the BEPs corresponding to different interfering signal power are relatively close, whereas the BEP differences become larger when the transmit power reaches 20 dBW.

Then, the influence of the kth user's own transmit power on BEP is analyzed. The experimental results in Fig. 11 demonstrate that with the increase of transmit power, the BEP of kth user increases. Taking the case of the channel parameter $\mu=2$ as an example, the BEP is smaller than 10^{-4} when the transmit power is 5 dBW, while it reaches nearly 10^{-2} as the transmit power arrives at 30 dBW. This can be interpreted by that the enhancement of transmit power would cause greater self-interference, which further affects the BEP. In addition, when the transmit power is fixed, the BEP decreases as the
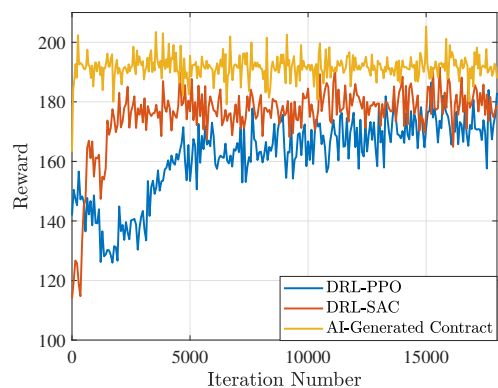
(a) Traning process, with diffusion step $N = 10$, batch size $N_b = 512$, discount factor $\gamma = 0.95$, soft target update parameter $\tau = 0.005$, exploration noise $\epsilon = 0.01$, contract generation network ε_θ learning rate is 10^{-5}, and contract quality network Q_v learning rate is 10^{-5}.
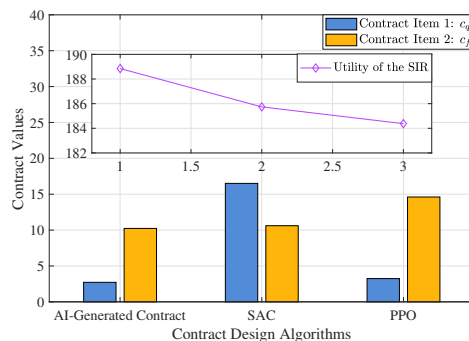
(b) The designed contracts, with $c_s = 1000$, $c_p = 0.03$, $D_{jk} = 6$ m, $\alpha = 4$, $\mu = 4$, $\beta_k = 12.9$, $\sigma_N^2 = \sigma_S^2 = 0.2$, $P_I = 3$ dBW, $\eta_k = 0.3$, $v_k = 0.2$, $B_{jk} = 10$ MHz, and $N = 3$.

Fig. 9. The effect of our proposed free-space sharing mechanism under different incentive design schemes, e.g., DRL-PPO, DRL-SAC, and AI-generated contract.

channel parameter increases, indicating that the severity of multipath effects directly impacts the kth user's BEP.
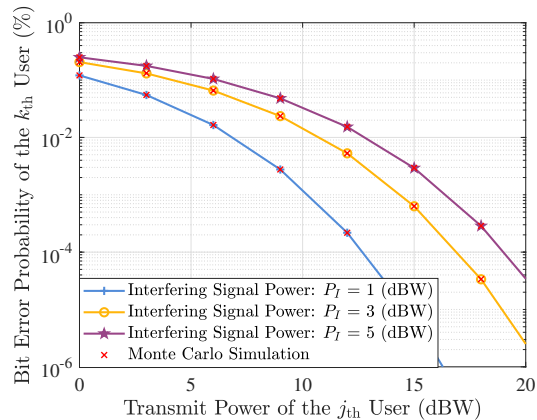
Fig. 10. The bit error probability of the kth user versus the transmit power of the jth user under different interfering signal power, with $D_{jk} = 5$ m, $\beta_k = 2$, $\alpha = 4$, $\mu = 5$, $\sigma_N^2 = \sigma_S^2 = 0.1$, $P_k = 20$ dBW, $P_I = 1$ dBW, $\eta_k = 0.2$, $v_k = 0.2$, and $N = 2$.

Fig. 12. The achievable rate of the kth user versus the transmit power of the jth user under different transmit distance, with $\beta_k = 2$, $\alpha = 4$, $\mu = 5$, $\sigma_N^2 = \sigma_S^2 = 0.8$, $P_j = 10$ dBW, $P_I = 1$ dBW, $\eta_k = 0.2$, $v_k = 0.2$, $B_{jk} = 10$ MHz and $N = 2$, under the full-duplex and half-duplex modes.
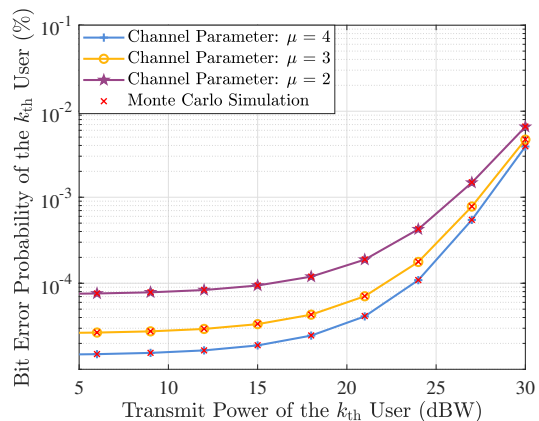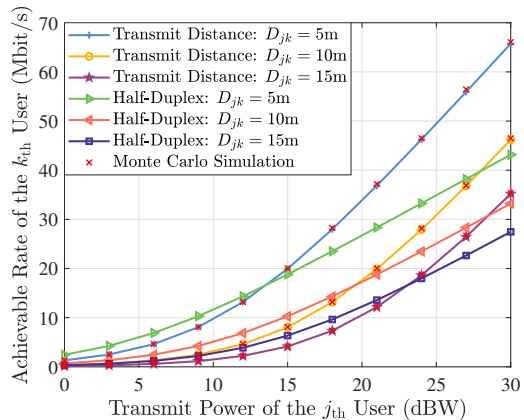

Fig. 11. The bit error probability of the kth user versus the transmit power of the kth user under different channel parameters, with $D_{jk} = 10$ m, $\beta_k = 2$, $\alpha = 4$, $\mu = 4$, $\sigma_N^2 = \sigma_S^2 = 0.1$, $P_j = 20$ dBW, $P_I = 1$ dBW, $\eta_k = 0.2$, $v_k = 0.2$, and $N = 2$.
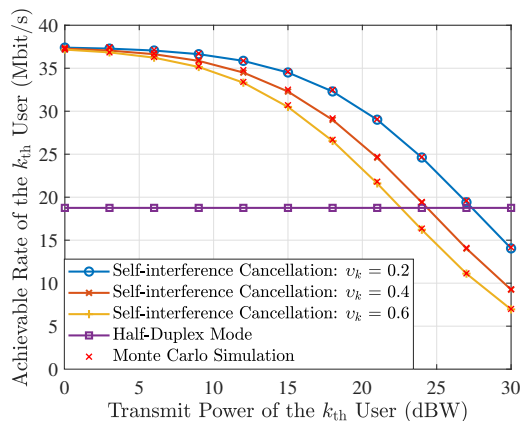

Fig. 13. The achievable rate of the kth user versus the transmit power of the kth user under different self-interference cancellation, with $D_{jk} = 5$ m, $\beta_k = 2$, $\alpha = 4$, $\mu = 5$, $\sigma_N^2 = \sigma_S^2 = 0.1$, $P_j = 10$ dBW, $P_I = 1$ dBW, $\eta_k = 0.2$, $B_{jk} = 10$ MHz and $N = 2$, under the full-duplex and half-duplex modes.

Next, under the condition of different distances between transmitter and receiver, the influence of transmit power on achievable rate is analyzed. From the results in Fig. 12, one can see that the achievable rate increases with the boost of the transmit power. For instance, when the distance between the SIP and SIR is 5 meters, the achievable rate is approximately 1 Mbit/s at 0 dBW, but it reaches 50 Mbit/s when the transmit power is increased to 25 dBW. The reason is that increasing transmit power raises the SINR. Conversely, increasing the distance between the transmitter and the receiver would lead to a decrease in the SINR. Furthermore, we compare the performance of full-duplex and half-duplex modes. Our results demonstrate that when the transmit power of the SI, i.e., the j^{th}user , is small, the achievable rate in full-duplex mode is lower than that in half-duplex mode due to the impact of strong self-interference. However, since the bandwidth can be shared, the increase in SIP's transmit power has a more significant impact on improving achievable rate in the full-duplex mode.

We proceed to investigate the impact of the kth user's own transmit power on the achievable rate and the results are shown in Fig. 13. Specifically, when v_k is fixed, increasing the transmit power of the kth user would cause a decrease to the achievable rate, since the power enhancement introduce greater self-interference. From another point of view, it can be seen that improving the interference cancellation technique, i.e., decreasing v_k, can enhance the achievable rate. In the half-duplex mode, the received achievable rate at the SIR's side is not affected by its own transmit power, as users do not transmit and receive data simultaneously. By comparing the full-duplex and half-duplex modes, we conclude that the half-duplex mode could achieve a higher achievable rate than the full-duplex mode when the user's own transmit power is higher and the self-interference cancellation technique is poor.

VII. CONCLUSION

We studied a D2D full-duplex communications system in which a free-space information-sharing mechanism was

proposed to avoid redundant computation tasks. Specifically, the semantic encoder in the SIP extracts semantic information, i.e., interest points and descriptors, from the view image. Computation results and semantic information are then transmitted to SIRs in full-duplex communication mode. We modeled the wireless channel using a generalized small-scale fading model and comprehensively analyzed the effects of self-interference and multiple co-channel interference signals. The closed-form achievable rate and BEP were derived. After the SIR receives the semantic information, it can perform semantic matching to save energy for redundant computation tasks. We proposed a contract-based mechanism to incentivize semantic information sharing. A novel diffusion model-based AI-generated contract design algorithm was proposed, achieving higher SIR utility than DRL-based algorithms. For future work, our proposed semantic information-sharing framework can be further enhanced by considering more accurate self-interference modeling. The proposed diffusion model-based algorithm holds promise for solving various optimization problems in wireless networks.

APPENDIX A
PROOF FOR LEMMA 1

A. Proof of the PDF expression

Because $|g_k|^2 \sim \text{Rayleigh}(\eta_k)$ and the sum of N i.i.d. Rayleigh-fading signals have a Nakagami-m distributed signal amplitude with $m = N$, the PDF and CDF expressions of $U \triangleq \sum_{i=1}^{N} |g_k|^2$ can be written as follows [52].

$$f_U(x) = \frac{x^{N-1}}{\eta_k^N \Gamma(N)} \exp\left(-\frac{x}{\eta_k}\right), \quad \text{(A-1)}$$

where $\eta_k = \mathbb{E}[g_k^2]$, and $\mathbb{E}[\cdot]$ denotes expectation.

Let $V \triangleq P_I U + \upsilon_k P_k \sigma_S^2 + \sigma_N^2$ and $\varphi \triangleq \upsilon_k P_k \sigma_S^2 + \sigma_N^2$. Then, the PDF of V can be derived as

$$f_V(y) = \frac{1}{P_I} f_U\left(\frac{y - \varphi}{P_I}\right). \quad \text{(A-2)}$$

Substituting (A-1) into (A-2), we have

$$f_V(y) = \frac{(y - \varphi)^{N-1}}{(P_I \eta_k)^N \Gamma(N)} \exp\left(-\frac{y - \varphi}{\eta_k P_I}\right). \quad \text{(A-3)}$$

Let $W \triangleq P_j D_{jk}^{-\beta_k} |h_{jk}|^2$. We can obtain that

$$f_W(w) = \frac{1}{P_j D_{jk}^{-\beta_k}} f_{|h_{jk}|^2}\left(\frac{w}{P_j D_{jk}^{-\beta_k}}\right) \quad \text{(A-4)}$$

By substituting (3) into (A-4), the PDF of W can be derived as

$$f_W(w) = \frac{\alpha(w)^{\frac{\alpha\mu}{2}-1}}{2\left(P_j D_{jk}^{-\beta_k} \beta\right)^{\frac{\alpha\mu}{2}} \Gamma(\mu)} \exp\left(-\left(\frac{w}{\beta P_j D_{jk}^{-\beta_k}}\right)^{\frac{\alpha}{2}}\right). \quad \text{(A-5)}$$

Because $\gamma_k = \frac{W}{V}$, we can derive the PDF of γ_k as

$$f_{\gamma_k}(x) = \int_0^\infty y f_W(xy) f_V(y) \, dy \quad \text{(A-6)}$$

Substituting (A-4) and (A-2) into (A-6), we have

$$f_{\gamma_k}(x) = \frac{\alpha x^{\frac{\alpha\mu}{2}-1}}{2\left(P_j D_{jk}^{-\beta_k} \beta\right)^{\frac{\alpha\mu}{2}} (P_I \eta_k)^N \Gamma(N) \Gamma(\mu)} I_1, \quad \text{(A-7)}$$

where

$$I_1 = \int_\varphi^\infty y^{\frac{\alpha\mu}{2}} (y - \varphi)^{N-1} \exp\left(-\frac{y - \varphi}{\eta_k P_I}\right)$$
$$\times \exp\left(-\left(\frac{xy}{\beta P_j D_{jk}^{-\beta_k}}\right)^{\frac{\alpha}{2}}\right) dy \quad \text{(A-8)}$$

To solve for the integral in I_1, we map the exponential function to the complex domain. According to [53, eq. (01.03.07.0001.01)] as a Mellin-Barnes integral

$$\exp\left(-\left(\frac{xy}{\beta P_j D_{jk}^{-\beta_k}}\right)^{\frac{\alpha}{2}}\right) = \int_{\mathcal{L}_1} \frac{\Gamma(s_1)}{2\pi i} \left(\frac{xy}{\beta P_j D_{jk}^{-\beta_k}}\right)^{\frac{-s_1\alpha}{2}} ds_1, \quad \text{(A-9)}$$

where the integration path of $\mathcal{L}_1$ goes from $s_1 - \infty j$ to $s_1 + \infty j$ and $s_1 \in \mathbb{R}$, and

$$\exp\left(-\frac{y - \varphi}{\eta_k P_I}\right) = \frac{1}{2\pi i} \int_{\mathcal{L}_2} \Gamma(s_2) \left(\frac{y - \varphi}{\eta_k P_I}\right)^{-s_2} ds_2, \quad \text{(A-10)}$$

where the integration path of $\mathcal{L}_2$ goes from $s_2 - \infty j$ to $s_2 + \infty j$ and $s_2 \in \mathbb{R}$. Substituting (A-9) and (A-10) into (A-8) and changing the order of integration, we can rewrite I_1 as

$$I_1 = \left(\frac{1}{2\pi i}\right)^2 \int_{\mathcal{L}_1} \int_{\mathcal{L}_2} \Gamma(s_1) \Gamma(s_2) \left(\frac{1}{\eta_k P_I}\right)^{-s_2}$$
$$\times \left(\frac{x}{\beta P_j D_{jk}^{-\beta_k}}\right)^{\frac{-s_1\alpha}{2}} I_2 ds_1 ds_2, \quad \text{(A-11)}$$

where

$$I_2 = \int_\varphi^\infty y^{\frac{\alpha\mu-s_1\alpha}{2}} (y - \varphi)^{N-1-s_2} dy \quad \text{(A-12)}$$

With the help of [34, eq. (3.191.2)], I_2 can be solved as

$$I_2 = \varphi^{N-s_2+\frac{\alpha\mu-s_1\alpha}{2}} B\left(s_2 - N - \frac{\alpha\mu - s_1\alpha}{2}, N - s_2\right), \quad \text{(A-13)}$$

where $B(\cdot, \cdot)$ denotes the beta function [34, eq. (8.38)]. Substituting (A-8) and (A-13) into (A-7) and using [34, eq. (8.384.1)], we can obtain the PDF expression of γ_k in the Mellin-Barnes integral as

$$f_{\gamma_k}(x) = \frac{\alpha x^{\frac{\alpha\mu}{2}-1} \varphi^{N+\frac{\mu}{2}\alpha}}{2\left(P_j D_{jk}^{-\beta_k} \beta\right)^{\frac{\alpha\mu}{2}} (P_I \eta_k)^N \Gamma(N) \Gamma(\mu)} \left(\frac{1}{2\pi i}\right)^2$$
$$\times \int_{\mathcal{L}_1} \int_{\mathcal{L}_2} \frac{\Gamma(s_1) \Gamma(s_2) \Gamma(N - s_2)}{\Gamma\left(\frac{s_1-\mu}{2}\alpha\right) \Gamma\left(s_2 - N + \frac{s_1-\mu}{2}\alpha\right)}$$
$$\times \left(\frac{\varphi}{\eta_k P_I}\right)^{-s_2} \left(\frac{\varphi x}{\beta P_j D_{jk}^{-\beta_k}}\right)^{\frac{-s_1\alpha}{2}} ds_1 ds_2 \quad \text{(A-14)}$$

Let $s_1 \triangleq t_1 + \mu$ and $s_2 \triangleq N - t_2$. With the help of [50, eq. (A-1)], the PDF of γ_k can be expressed in form of the

Multivariate Fox's H-function as (24) to complete the proof.

B. Proof of the CDF expression

With the help of the definition of CDF, we have

$$F_{\gamma_k}(x) = \int_0^x f_{\gamma_k}(y)\,\mathrm{d}y \qquad \text{(A-15)}$$

Substituting (24) into (A-15) and using [50, eq. (A-1)], we can re-write the CDF of γ_k as

$$F_{\gamma_k}(x) = \frac{\alpha(2\pi i)^{-2}}{2\Gamma(N)\Gamma(\mu)} \int_{\mathcal{L}_1}\int_{\mathcal{L}_2} \frac{\Gamma(t_1+\mu)\Gamma(t_2)\Gamma(N-t_2)}{\Gamma\left(\frac{\alpha}{2}t_1-t_2\right)\Gamma\left(\frac{\alpha}{2}t_1\right)}$$

$$\times \left(\frac{\varphi}{\beta P_j D_{jk}^{-\beta_k}}\right)^{\frac{-\alpha}{2}t_1} \left(\frac{\varphi}{\eta_k P_I}\right)^{t_2} I_3\,\mathrm{d}t_1\mathrm{d}t_2, \qquad \text{(A-16)}$$

where I_3 can be solved by using [34, eq. (8.334.3)] as

$$I_3 = \int_0^x y^{\frac{-\alpha}{2}t_1-1}\mathrm{d}y = \frac{\Gamma\left(-\frac{\alpha}{2}t_1\right)}{\Gamma\left(1-\frac{\alpha}{2}t_1\right)} x^{\frac{-\alpha}{2}t_1}. \qquad \text{(A-17)}$$

By substituting I_3 into (A-16) and using [50, eq. (A-1)], the CDF of γ_k can be derived as (25), which completes the proof.

APPENDIX B
PROOF FOR LEMMA 2

A. Proof of the PDF expression

With the help of (A-7) and (A-9), we can express the PDF of $\gamma_{k'}$ as

$$f_{\gamma_{k'}}(x) = \frac{\alpha x^{\frac{\alpha\mu}{2}-1}}{2\left(P_j D_{jk}^{-\beta_k}\beta\right)^{\frac{\alpha\mu}{2}}(P_I\eta_k)^N\Gamma(N)\Gamma(\mu)} I_B, \qquad \text{(B-1)}$$

where

$$I_B = \int_{\mathcal{L}_1} \frac{\Gamma(s_1)}{2\pi i}\left(\frac{x}{\beta P_j D_{jk}^{-\beta_k}}\right)^{\frac{-s_1\alpha}{2}}$$

$$\times \int_0^\infty y^{\frac{\alpha\mu}{2}+N-1-\frac{s_1\alpha}{2}}\exp\left(-\frac{y}{\eta_k P_I}\right)\mathrm{d}y\mathrm{d}s_1 \qquad \text{(B-2)}$$

Using [34, eq. (3.351.3)], we can solve the integration in I_B. Substituting I_B into (B-1) and using [50, eq. (A-1)], we derive the PDF as (27).

B. Proof of the CDF expression

According to the definition of CDF and (27), we have

$$F_{\gamma_k}(x) = \frac{\alpha(\eta_k P_I)^{\frac{\alpha\mu}{2}}\Gamma^{-1}(\mu)}{2\left(P_j D_{jk}^{-\beta_k}\beta\right)^{\frac{\alpha\mu}{2}}\Gamma(N)} \int_{\mathcal{L}_1} \Gamma\left(\frac{\alpha(\mu-s_1)}{2}+N\right)$$

$$\times \frac{\Gamma(s_1)}{2\pi i}\left(\frac{\eta_k P_I}{\beta P_j D_{jk}^{-\beta_k}}\right)^{\frac{-s_1\alpha}{2}} \int_0^x y^{\frac{\alpha\mu}{2}-1-\frac{s_1\alpha}{2}}\mathrm{d}y\mathrm{d}s_1, \qquad \text{(B-3)}$$

where

$$\int_0^x y^{\frac{\alpha\mu}{2}-1-\frac{s_1\alpha}{2}}\mathrm{d}y = \frac{\Gamma\left(\frac{\alpha\mu}{2}-\frac{s_1\alpha}{2}\right)}{\Gamma\left(\frac{\alpha\mu}{2}-\frac{s_1\alpha}{2}+1\right)} y^{\frac{\alpha\mu}{2}-\frac{s_1\alpha}{2}}. \qquad \text{(B-4)}$$

Substituting (B-4) into (B-3) and using [50, eq. (A-1)], we derive the CDF as (28).

APPENDIX C
PROOF FOR THEOREM 1

Substituting (24) into (30), we can express the achievable rate as

$$C_k = \frac{\Gamma^{-1}(\mu)\alpha}{2\Gamma(N)}\left(\frac{1}{2\pi i}\right)^2 \int_{\mathcal{L}_1}\int_{\mathcal{L}_2} \frac{\Gamma(t_1+\mu)\Gamma(t_2)\Gamma(N-t_2)}{\Gamma\left(\frac{\alpha}{2}t_1-t_2\right)\Gamma\left(\frac{\alpha}{2}t_1\right)}$$

$$\times I_4\left(\frac{\varphi}{\beta P_j D_{jk}^{-\beta_k}}\right)^{\frac{-\alpha}{2}t_1}\left(\frac{\varphi}{\eta_k P_I}\right)^{t_2}\mathrm{d}t_1\mathrm{d}t_2 \qquad \text{(C-1)}$$

where

$$I_4 = \int_0^\infty y^{\frac{-\alpha}{2}t_1-1}\log_2(1+y)\,\mathrm{d}y. \qquad \text{(C-2)}$$

With the help of [54, eq. (2.6.9.21)] and [34, eq. (8.334.3)], I_4 can be deduced as

$$I_4 = \frac{\pi\csc\left(\pi\frac{\alpha}{2}t_1\right)}{\frac{\alpha}{2}t_1\ln 2} = \frac{\Gamma\left(1-\frac{\alpha}{2}t_1\right)\Gamma^2\left(\frac{\alpha}{2}t_1\right)}{\Gamma\left(1+\frac{\alpha}{2}t_1\right)\ln 2} \qquad \text{(C-3)}$$

Substituting I_4 into (C-1) and using [50, eq. (A-1)], we can derive the achievable rate as (31) to complete the proof.

APPENDIX D
PROOF FOR THEOREM 2

Using the definition of Gamma function [34, eq. (8.350)], we can re-write E_k as

$$E_k = \frac{\tau_1^{\tau_2}}{2\Gamma(\tau_2)}\int_0^\infty x^{\tau_2-1}e^{-\tau_1 x}F_{\gamma_k}(x)\,\mathrm{d}x. \qquad \text{(D-1)}$$

Substituting (25) into (D-1), we obtain

$$E_k = \int_{\mathcal{L}_1}\int_{\mathcal{L}_2} \frac{\Gamma(t_1+\mu)\Gamma\left(-\frac{\alpha}{2}t_1\right)\Gamma(t_2)\Gamma(N-t_2)}{\Gamma\left(\frac{\alpha}{2}t_1-t_2\right)\Gamma\left(\frac{\alpha}{2}t_1\right)\Gamma\left(1-\frac{\alpha}{2}t_1\right)} I_5$$

$$\times\frac{\alpha\tau_1^{\tau_2}\Gamma^{-1}(\tau_2)}{4\Gamma(N)\Gamma(\mu)}\left(\frac{1}{2\pi i}\right)^2\left(\frac{D_{jk}^{\beta_k}\varphi}{\beta P_j}\right)^{\frac{-\alpha}{2}t_1}\left(\frac{\varphi}{\eta_k P_I}\right)^{t_2}\mathrm{d}t_1\mathrm{d}t_2 \qquad \text{(D-2)}$$

where

$$I_5 = \int_0^\infty x^{\frac{-\alpha}{2}t_1+\tau_2-1}e^{-\tau_1 x}\mathrm{d}x. \qquad \text{(D-3)}$$

With the help of [34, eq. (3.351.3)] and [34, eq. (8.339.1)], I_D can be solved as

$$I_5 = \tau_1^{\frac{\alpha}{2}t_1-\tau_2}\Gamma\left(\tau_2-\frac{\alpha}{2}t_1\right). \qquad \text{(D-4)}$$

Substituting I_5 into (D-2) and using [50, eq. (A-1)], we can derive 33 to complete the proof.

REFERENCES

[1] Z. Li, H. Zhou, T. Zhou, H. Yu, Z. Xu, and G. Sun, "Esync: Accelerating intra-domain federated learning in heterogeneous data centers," *IEEE Trans. Serv. Comput.*, vol. 15, no. 4, pp. 2261–2274, Apr. 2020.

[2] Y. Wang, Z. Su, N. Zhang, R. Xing, D. Liu, T. H. Luan, and X. Shen, "A survey on metaverse: Fundamentals, security, and privacy," *IEEE Commun. Surveys Tuts.*, to appear, 2022.

[3] H. Du, Z. Li, D. Niyato, J. Kang, Z. Xiong, D. I. Kim *et al.*, "Enabling AI-generated content (AIGC) services in wireless edge networks," *arXiv preprint arXiv:2301.03220*, 2023.

[4] D.-I. Han, M. C. tom Dieck, and T. Jung, "User experience model for augmented reality applications in urban heritage tourism," *J. Heritage Tour.*, vol. 13, no. 1, pp. 46–61, Jan. 2018.

[5] W. Yang, H. Du, Z. Q. Liew, W. Y. B. Lim, Z. Xiong, D. Niyato, X. Chi, X. S. Shen, and C. Miao, "Semantic communications for future Internet: Fundamentals, applications, and challenges," *IEEE Commun. Surveys Tuts.*, to appear, 2022.

[6] Z. Li, Y. He, H. Yu, J. Kang, X. Li, Z. Xu, and D. Niyato, "Data heterogeneity-robust federated learning via group client selection in industrial iot," *IEEE Internet Things J.*, vol. 9, no. 18, pp. 17 844–17 857, 2022.

[7] Y. Zhang, M. Pan, L. Song, Z. Dawy, and Z. Han, "A survey of contract theory-based incentive mechanism design in wireless networks," *IEEE Wireless Commun.*, vol. 24, no. 3, pp. 80–85, Mar. 2017.

[8] H. Du, J. Liu, D. Niyato, J. Kang, Z. Xiong, J. Zhang, and D. I. Kim, "Attention-aware resource allocation and QoE analysis for metaverse xURLLC services," *arXiv preprint arXiv:2208.05438*, 2022.

[9] D. Silver, A. Huang, C. J. Maddison, A. Guez, L. Sifre, G. Van Den Driessche, J. Schrittwieser, I. Antonoglou, V. Panneershelvam, M. Lanctot *et al.*, "Mastering the game of Go with deep neural networks and tree search," *Nature*, vol. 529, no. 7587, pp. 484–489, 2016.

[10] P. Garnier, J. Viquerat, J. Rabault, A. Larcher, A. Kuhnle, and E. Hachem, "A review on deep reinforcement learning for fluid mechanics," *Comput. Fluids*, vol. 225, p. 104973, 2021.

[11] H. Alves, T. Riihonen, and H. A. Suraweera, *Full-Duplex Communications for Future Wireless Networks*. Springer, 2020.

[12] D. Kim, H. Lee, and D. Hong, "A survey of in-band full-duplex transmission: From the perspective of PHY and MAC layers," *IEEE Commun. Surv. Tut.*, vol. 17, no. 4, pp. 2017–2046, Apr. 2015.

[13] K. E. Kolodziej, B. T. Perry, and J. S. Herd, "In-band full-duplex technology: Techniques and systems survey," *IEEE Trans. Microw. Theory Tech.*, vol. 67, no. 7, pp. 3025–3041, July 2019.

[14] L. Han, Y. Zhang, X. Zhang, and J. Mu, "Power control for full-duplex D2D communications underlaying cellular networks," *IEEE Access*, vol. 7, pp. 111 858–111 865, 2019.

[15] K. S. Ali, H. ElSawy, and M.-S. Alouini, "Modeling cellular networks with full-duplex D2D communication: A stochastic geometry approach," *IEEE Trans. Commun.*, vol. 64, no. 10, pp. 4409–4424, Oct. 2016.

[16] F. Liu, X. Hou, and Y. Liu, "Capacity improvement for full duplex device-to-device communications underlaying cellular networks," *IEEE Access*, vol. 6, pp. 68 373–68 383, 2018.

[17] N. Lee, X. Lin, J. G. Andrews, and R. W. Heath, "Power control for D2D underlaid cellular networks: Modeling, algorithms, and analysis," *IEEE J. Sel. Areas Commun.*, vol. 33, no. 1, pp. 1–13, Jan 2014.

[18] D. Feng, L. Lu, Y. Yuan-Wu, G. Y. Li, G. Feng, and S. Li, "Device-to-device communications underlaying cellular networks," *IEEE Trans. Commun.*, vol. 61, no. 8, pp. 3541–3551, Aug. 2013.

[19] A. J. Davison, I. D. Reid, N. D. Molton, and O. Stasse, "MonoSLAM: Real-time single camera SLAM," *IEEE Trans. Pattern Anal. Mach. Intell.*, vol. 29, no. 6, pp. 1052–1067, Jun. 2007.

[20] R. Mur-Artal, J. M. M. Montiel, and J. D. Tardos, "ORB-SLAM: a versatile and accurate monocular SLAM system," *IEEE Trans. Robot.*, vol. 31, no. 5, pp. 1147–1163, May 2015.

[21] J. Engel, V. Koltun, and D. Cremers, "Direct sparse odometry," *IEEE Trans. Pattern Anal. Mach. Intell.*, vol. 40, no. 3, pp. 611–625, Mar. 2017.

[22] L. Xiao, J. Wang, X. Qiu, Z. Rong, and X. Zou, "Dynamic-SLAM: Semantic monocular visual localization and mapping based on deep learning in dynamic environment," *Robotics and Autonomous Systems*, vol. 117, pp. 1–16, 2019.

[23] Z. Wang, Q. Zhang, J. Li, S. Zhang, and J. Liu, "A computationally efficient semantic slam solution for dynamic scenes," *Remote Sens.*, vol. 11, no. 11, p. 1363, Nov. 2019.

[24] D. DeTone, T. Malisiewicz, and A. Rabinovich, "Superpoint: Self-supervised interest point detection and description," in *Proc. IEEE Conf. Comput. Vis. Pattern Recognit.*, 2018, pp. 224–236.

[25] P.-E. Sarlin, D. DeTone, T. Malisiewicz, and A. Rabinovich, "Superglue: Learning feature matching with graph neural networks," in *Proc. IEEE Conf. Comput. Vis. Pattern Recognit.*, 2020, pp. 4938–4947.

[26] P. A. Rauschnabel, "Augmented reality is eating the real-world! The substitution of physical products by holograms," *Int. J. Inf. Mana.*, vol. 57, p. 102279, 2021.

[28] T. Vojir, T. Šipka, R. Aljundi, N. Chumerin, D. O. Reino, and J. Matas, "Road anomaly detection by partial image reconstruction with segmentation coupling," in *Proc. IEEE Conf. Comput. Vis. Pattern Recognit.*, 2021, pp. 15 651–15 660.

[27] C. Kerdvibulvech, "Exploring the impacts of COVID-19 on digital and metaverse games," in *Int. Conf. Hum. Comput. Int.*, 2022, pp. 561–565.

[29] D. H. Kong, Y.-S. Kil, and S.-H. Kim, "Neural network aided digital self-interference cancellation for full-duplex communication over time-varying channels," *IEEE Trans. Veh. Technol.*, vol. 71, no. 6, pp. 6201–6213, Jun. 2022.

[30] L. Han, Y. Zhang, Y. Li, and X. Zhang, "Spectrum-efficient transmission mode selection for full-duplex-enabled two-way D2D communications," *IEEE Access*, vol. 8, pp. 115 982–115 991, 2020.

[31] H. Gao, P. J. Smith, and M. V. Clark, "Theoretical reliability of MMSE linear diversity combining in rayleigh-fading additive interference channels," *IEEE Trans. Commun.*, vol. 46, no. 5, pp. 666–672, May 1998.

[32] J. Kang, H. Du, Z. Li, Z. Xiong, S. Ma, D. Niyato, and Y. Li, "Personalized saliency in task-oriented semantic communications: Image transmission and performance analysis," *IEEE J. Sel. Areas Commun.*, vol. 41, no. 1, pp. 186–201, Jan. 2022.

[33] M. D. Yacoub, "The α-μ distribution: A physical fading model for the stacy distribution," *IEEE Trans. Veh. Tech.*, vol. 56, no. 1, pp. 27–34, Jan. 2007.

[34] I. S. Gradshteyn and I. M. Ryzhik, *Table of Integrals, Series, and Products*, 7th ed. Academic Press, 2007.

[35] S. Ji, S. Pan, E. Cambria, P. Marttinen, and S. Y. Philip, "A survey on knowledge graphs: Representation, acquisition, and applications," *IEEE Trans. Neural Networks Learn. Syst.*, vol. 33, no. 2, pp. 494–514, Feb. 2021.

[36] W. C. Ng, H. Du, W. Y. B. Lim, Z. Xiong, D. Niyato, and C. Miao, "Stochastic resource allocation for semantic communication-aided virtual transportation networks in the metaverse," *arXiv preprint arXiv:2208.14661*, 2022.

[37] X. Kang, B. Song, J. Guo, Z. Qin, and F. R. Yu, "Task-oriented image transmission for scene classification in unmanned aerial systems," *IEEE Trans. Commun.*, vol. 70, no. 8, pp. 5181–5192, Aug. 2022.

[38] K. Simonyan and A. Zisserman, "Very deep convolutional networks for large-scale image recognition," *arXiv preprint arXiv:1409.1556*, 2014.

[39] A. Odena, V. Dumoulin, and C. Olah, "Deconvolution and checkerboard artifacts," *Distill*, vol. 1, no. 10, p. e3, Oct. 2016.

[40] C. B. Choy, J. Gwak, S. Savarese, and M. Chandraker, "Universal correspondence network," *Proc. Adv. Neural Inf. Process. Syst.*, vol. 29, 2016.

[41] T. Trzcinski, J. Komorowski, L. Dabala, K. Czarnota, G. Kurzejamski, and S. Lynen, "Scone: Siamese constellation embedding descriptor for image matching," in *Proc. Eur. Conf. Comput. Vis.*, 2018, pp. 0–0.

[42] M. M. Chun, "Contextual cueing of visual attention," *Trends Cogn. Sci.*, vol. 4, no. 5, pp. 170–178, May 2000.

[43] J. Gehring, M. Auli, D. Grangier, D. Yarats, and Y. N. Dauphin, "Convolutional sequence to sequence learning," in *Proc. Int. Conf. Mach. Learn.* PMLR, 2017, pp. 1243–1252.

[44] G. Peyré and M. Cuturi, "Computational optimal transport," *Found. Trends Mach. Learn.*, vol. 11, no. 5-6, pp. 355–607, 2019.

[45] T. Nishio, R. Shinkuma, T. Takahashi, and N. B. Mandayam, "Service-oriented heterogeneous resource sharing for optimizing service latency in mobile cloud," in *Proc. Int. Mobile Cloud Comput. & Netw. Workshop*, 2013, pp. 19–26.

[46] Y. Zhang, Y. Gu, M. Pan, N. H. Tran, Z. Dawy, and Z. Han, "Multi-dimensional incentive mechanism in mobile crowdsourcing with moral hazard," *IEEE Trans. Mobile Comput.*, vol. 17, no. 3, pp. 604–616, Mar. 2017.

[47] Y. Zhang and Z. Han, *Contract Theory for Wireless Networks*. Springer, 2017.

[48] J. Ho, A. Jain, and P. Abbeel, "Denoising diffusion probabilistic models," *Proc. Adv. Neural Inf. Process. Syst.*, vol. 33, pp. 6840–6851, 2020.

[49] H. Hasselt, "Double Q-learning," *Proc. Adv. Neural Inf. Process. Syst.*, vol. 23, 2010.

[50] A. M. Mathai, R. K. Saxena, and H. J. Haubold, *The H-function: Theory and Applications*. Springer Science & Business Media, 2009.

[51] D. Tse and P. Viswanath, *Fundamentals of wireless communication*. Cambridge university press, 2005.

[52] M. Nakagami, "The m-distribution—A general formula of intensity distribution of rapid fading," in *Stat. Methods Radio Wave Propag.*, 1960, pp. 3–36.

[53] Wolfram, "The wolfram functions site," http://functions.wolfram.com.

[54] A. P. Prudnikov, J. A. Bryčkov, and O. I. Maričev, *Integrals and Series. Vol. 1, Elementary Function*, 1986.